Thesis for the degree of Doctor of Philosophy

Nonlinear intrachannel distortion in high-speed optical transmission systems

Pontus Johannisson

CHALMERS

Department of Radio and Space Science
Chalmers University of Technology
Göteborg, Sweden, 2006

Nonlinear intrachannel distortion in high-speed optical transmission systems

Pontus Johannisson

ISBN 91-7291-843-8
Doktorsavhandlingar vid Chalmers tekniska högskola
Ny serie nr 2525
ISSN 0346-718X

Department of Radio and Space Science
Chalmers University of Technology
SE–412 96 Göteborg
Sweden
Telephone +46–(0)31–772 10 00

Printed in Sweden by
Reproservice
Chalmers Tekniska Högskola
Göteborg, Sweden, 2006

Nonlinear intrachannel distortion in high-speed optical transmission systems

Pontus Johannisson
Department of Radio and Space Science
Chalmers University of Technology

Abstract

The Kerr nonlinearity in optical fibres tends to generate signal distortion in dispersion-managed fibre-optic communication systems. Within a wavelength channel, the resulting intrachannel effects are timing jitter, i.e., random temporal shifting of the signal pulses, amplitude jitter, and generation of noise pulses in empty bit slots, referred to as ghost pulses. An investigation of these effects is carried out using both a variational and a perturbation analysis of the nonlinear Schrödinger equation. This allows the nonlinear interaction to be described analytically and numerical simulations are presented that support and extend the obtained results.

The interaction range, i.e., the number of bit slots over which the nonlinear interaction is significant, is an important concept when designing and interpreting system simulations. Analytical and numerical results are given which allow *a priori* estimations valid for realistic systems. The growth rate of the nonlinear distortion has been examined in order to investigate the possibilities for suppressing the nonlinear interaction.

Methods for counteracting the nonlinear effects are proposed, and special emphasis is given to the suppressive effects obtained from phase shifting of consecutive signal pulses. All-optical regeneration is discussed as an alternative method of reducing the signal distortion and in particular two types of regenerators are studied. The first type is based on nonlinear spectral widening and bandpass filtering and is suitable for return-to-zero data. The second type can reduce the phase fluctuations in differential phase-shift keying data and the analysis provides a description of an already experimentally implemented device.

Keywords: nonlinear optics, fibre optics, self-phase modulation, cross-phase modulation, intrachannel four-wave mixing, timing jitter, ghost pulses, all-optical regeneration

Publications

This thesis is based on the work contained in the following papers:

[A] J. Mårtensson, A. Berntson, M. Westlund, A. Danielsson, P. Johannisson, D. Anderson, and M. Lisak, "Timing jitter owing to intrachannel pulse interactions in dispersion-managed transmission systems", *Opt. Lett.*, **26**, 2, 55–57, Jan 2001.

[B] P. Johannisson, D. Anderson, A. Berntson, and J. Mårtensson, "Generation and dynamics of ghost pulses in strongly dispersion-managed fiber-optic communication systems", *Opt. Lett.*, **26**, 16, 1227–1229, Aug 2001.

[C] P. Johannisson, "Interaction range and generation rate of nonlinear intrachannel signal distortion", *submitted to J. Opt. Soc. Am. B*, 2006.

[D] P. Johannisson, D. Anderson, M. Marklund, A. Berntson, M. Forzati, and J. Mårtensson, "Suppression of nonlinear effects by phase alternation in strongly dispersion-managed optical transmission", *Opt. Lett.*, **27**, 12, 1073–1075, June 2002.

[E] M. Forzati, J. Mårtensson, A. Berntson, A. Djupsjöbacka, and P. Johannisson, "Reduction of intrachannel four-wave mixing using the alternate-phase RZ modulation format", *IEEE Photon. Technol. Lett.*, **14**, 9, 1285–1287, Sept 2002.

[F] P. Johannisson and M. Karlsson, "Characterization of a self-phase-modulation-based all-optical regeneration system", *IEEE Photon. Technol. Lett.*, **17**, 12, 2667–2669, Dec 2005.

[G] P. Johannisson, G. Adolfsson, and M. Karlsson, "Suppression of phase error in differential phase-shift keying data by amplitude regeneration", *Opt. Lett.*, **31**, 10, 1385–1387, May 2006.

Related work by the author (not included in this thesis):

[H] G. Brodin, L. Stenflo, D. Anderson, M. Lisak, M. Marklund, and P. Johannisson, "Light bullets and optical collapse in vacuum", *Physics Letters A*, **306**, 4, 206–210, Jan 2003.

[I] P. Johannisson, D. Anderson, M. Lisak, and M. Marklund, "Nonlinear Bessel beams", *Opt. Commun.*, **222**, 107–115, July 2003.

[J] P. Johannisson, D. Anderson, M. Lisak, M. Marklund, R. Fedele, A. Kim, "Nonlocal effects in high-energy charged-particle beams", *Phys. Rev. E*, **69**, 066501:1–066501:7, June 2004.

[K] C.-J. Rosenberg, D. Anderson, M. Desaix, P. Johannisson, and M. Lisak, "Diffusion of super-Gaussian profiles", *submitted to Eur. J. Phys.*, 2006.

[L] C.-J. Rosenberg, D. Anderson, M. Desaix, P. Johannisson, and M. Lisak, "Evolution of optical pulses towards wave breaking in highly nonlinear fibres", *submitted to Opt. Commun.*, 2006.

Conference contributions by the author (not included in this thesis):

[M] P. Johannisson, D. Anderson, A. Berntson, and J. Mårtensson, "Perturbational analysis of the generation of ghost pulses in 40 Gbit/s fibre-optic communication systems", in *Nonlinear Guided Waves and Their Applications (NLGW 2001)*, MC74:1–MC74:3, March 2001.

[N] P. Johannisson, D. Anderson, A. Berntson, and J. Mårtensson, "Nonlinear generation of ghost pulses in high speed dispersion-managed communication systems", in *Optik i Sverige 2001*, PO22, Nov 2001.

[O] D. Anderson, P. Johannisson, M. Lisak, M. Marklund, J. Dudley, J. Harvey, R. Kruhlak, A. Peacock, and E. Vanin, "Pulse dynamics in optical amplifiers in the presence of bandwidth limitation and nonlinear gain saturation", in *Radiovetenskap och Kommunikation (RVK 2002) on CD*, 761–764, June 2002.

[P] P. Johannisson, D. Anderson, M. Marklund, A. Berntson, M. Forzati, and J. Mårtensson, "Suppression of nonlinear effects by phase alternation in dispersion managed optical fibre transmission", in *Radiovetenskap och Kommunikation (RVK 2002) on CD*, 770–773, June 2002.

[Q] D. Anderson, M. Lisak, M. Marklund, P. Johannisson, G. Brodin, and L. Stenflo, "Collapse of optical vacuum pulses due to QED nonlinearities", in *Nonlinear Guided Waves and Their Applications (NLGW 2002)*, NLMD27:1–NLMD27:3, Sept 2002.

[R] P. Johannisson, D. Anderson, M. Marklund, A. Berntson, M. Forzati, and J. Mårtensson, "Suppression of nonlinear effects by phase alternation in strongly dispersion-managed optical transmission", in *Nonlinear Guided Waves and Their Applications (NLGW 2002)*, NLTuD17:1–NLTuD17:3, Sept 2002.

[S] P. Johannisson, D. Anderson, R. Fedele, A. Kim, M. Lisak, and M. Marklund, "Analysis of pulse and shock dynamics in high energy charged particle beams using the thermal wave model", in *International Topical Conference on Plasma Physics*, PI:1, Sept 2003.

[T] P. Johannisson, D. Anderson, M. Lisak, and M. Marklund, "Nonlinear dynamics of Bessel beams", in *International Topical Conference on Plasma Physics*, PI:22, Sept 2003.

[U] P. Johannisson, D. Anderson, and M. Lisak, "Nonlinear intrachannel effects in fibre-optic communication systems", in *Northern Optics 2006*, 006, June 2006.

[V] P. Johannisson, G. Adolfsson, and M. Karlsson, "Phase regeneration of DPSK modulated data using averaging", in *Northern Optics 2006*, 005, June 2006.

Contents

Acknowledgement

I want to thank Prof. Dan Anderson and Prof. Mietek Lisak for accepting me as a Ph. D. student, for all their support, and for creating such a friendly and inspiring atmosphere in the group. A special thank goes to Prof. Mattias Marklund and Prof. Magnus Karlsson who have spent a lot of time helping me and discussing problems. The collaboration with Dr. Anders Berntson and his colleagues at Acreo has been invaluable, since it has defined the scope of this thesis and lead to a number of publications. I am grateful to have such friendly colleagues, among those Ulf Jordan who has taught me a million things about GNU/Linux and Andreas Fhager and Håkan Smith who are my friends since many years. Finally, I want to thank my family, Jenny, Alva, and Elias.

Acronyms

ACRZ	alternate-chirp return-to-zero
AMI	alternate-mark inversion
APRZ	alternate-phase return-to-zero
BER	bit-error rate
CD	chromatic dispersion
CRZ	chirped return-to-zero
CSRZ	carrier-suppressed return-to-zero
DB	duobinary
DCF	dispersion-compensating fibre
DI	delay interferometer
DM	dispersion-managed
DMF	data modulation format
DPSK	differential phase-shift keying
FWHM	full width at half maximum
FWM	four-wave mixing
GVD	group-velocity dispersion
HNLF	highly nonlinear fibre
NLSE	nonlinear Schrödinger equation
NOLM	nonlinear optical-loop mirror
NRZ	nonreturn-to-zero
OOK	on–off keying
OSNR	optical signal-to-noise ratio
PAPRZ	pairwise alternate-phase return-to-zero
PMD	polarisation-mode dispersion
PRBS	pseudorandom bit sequence
RZ	return-to-zero
SA	saturable absorber
SMF	standard monomode fibre
SOA	semiconductor optical amplifier

SORA	semiconductor optical regenerative amplifier
SPM	self-phase modulation
TDM	time-division multiplexing
TOD	third-order dispersion
WDM	wavelength-division multiplexing
XPM	cross-phase modulation

Chapter 1

Introduction

The demand for high-speed digital connections is ever increasing and optical fibres provide the best alternative for long-distance communication at high data rates [1]. The basic reason for this is the high frequency of light, which allows optical transmission systems to utilise a very large bandwidth. The rapid progress of the field has been made possible by the development of a number of key technologies [2]. One of these is optical amplification which can be done either in lumped form with a fibre amplifier, which basically is a doped and optically pumped piece of fibre, or in distributed form using Raman amplification [3]. The quality of optical communication fibres has also been significantly improved. One example is that the attenuation has been made extremely low, and the remaining losses are caused by fundamental physical limitations such as Rayleigh scattering. Communication fibres are also designed to operate in single-mode, i.e., they allow only one mode to propagate. This leads to small dispersive effects, but the invention of the dispersion-compensating fibre (DCF), which has chromatic dispersion (CD) with opposite sign as compared to the standard monomode fibre (SMF), marks another milestone. When combined these two types of fibres provide a tool to compensate for the CD in communication systems, enabling a technique known as *dispersion management*. Fibre amplifiers and dispersion management have together essentially eliminated the two significant obstacles of loss and CD, and have made a great increase of the transmission speed possible. However, as the data rate is further increased new effects become limiting factors.

One of the main constraints of current systems is that electronic devices are incapable of the high-speed light manipulation needed to take

full advantage of optical fibres. It is therefore routine to use *wavelength-division multiplexing* (WDM), where a number of channels are transmitted simultaneously through the same fibre by using a number of lasers operating at different wavelengths. When WDM is used the data rate becomes much higher in the fibre than in the electronic devices. However, the data rate per channel will still be dictated by the electronic equipment, and this requires the use of many lasers to provide light at the different channel wavelengths. To avoid this *time-division multiplexing* (TDM) can be used. A number of electric signals are then multiplexed into one single optical wavelength channel by packing the data more densely in time, thus reaching a significantly higher channel speed in the fibre than in the electronic equipment. However, these high data rates lead to a need for all-optical solutions for switching and (de-)multiplexing, and the design of these is non-trivial.

There are a number of physical effects that influence the light during the propagation through the fibre. Typically these will degrade the signal quality and lead to different constraints such as, e.g., a maximum transmission distance. It is, however, hard to find a general answer to the question which effect that is the limiting one, since this depends to a large extent on system parameters, such as type of fibre, bit rate, modulation format, power level, and type of filtering.

A full overview of the signal degrading effects is too complicated to be provided here, but at the channel speed of most concern to the present thesis (40 Gbit/s) the main effects include the following: Noise generation during amplification is a fundamental physical phenomenon which cannot be avoided. Thus the amplifier spacing is an important parameter since a small spacing leads to excessive noise generation and a large spacing leads to a low optical signal-to-noise ratio (OSNR) before the amplifier. It was mentioned above that dispersion management cancels the effect from CD, but this is not strictly true. The dispersion relation in a fibre is described by a Taylor expansion around the carrier frequency, and dispersion management can (in its usual form) only compensate for the impact from the second order term in this expansion (known as the *group-velocity dispersion* (GVD)). The next term in the expansion gives rise to *third-order dispersion* (TOD), and when the bit rates are increased and GVD is properly compensated for it may be necessary to take TOD into account. Another major issue is *polarisation-mode dispersion* (PMD). Even in an SMF there are two possible modes, since the polarisation of the field can be chosen as one

of the two possible orthogonal polarisation states. In a practical context these eigenmodes are not degenerated since no fibre is perfectly cylindrical. These modes will therefore propagate with different group velocities and this gives rise to pulse broadening [4]. The amount of PMD varies with, e.g., temperature and mechanical strain of the fibre and is difficult to compensate for.

In addition to the above mentioned effects there are also a number of nonlinear effects, and the presence of these is made obvious by the fact that for a given system there exists an optimum launch power [5,6]. This is easily understood since a low launch power leads to low OSNR and a high launch power leads to strong nonlinear signal distortion. The present thesis deals with effects that originate from the Kerr nonlinearity of the fibre.

The nonlinear distortion can be classified into interchannel effects, i.e., interaction between different channels in a WDM system, and intrachannel effects, which are present within each wavelength channel. The relative significance of these two classes depend on the bit rate and the amount of CD, but at channel speeds of the order of 40 Gbit/s and above, the intrachannel effects typically dominate [1], and they are the focus of the present thesis.

The strength of the nonlinear interaction also depends on the data modulation format, and this will be discussed in Chapter 6. In the preceding chapters the modulation format is assumed to be return-to-zero (RZ) on–off keying (OOK). The reason for this choice is that data with RZ modulation has a better tolerance to nonlinear effects than nonreturn-to-zero (NRZ) data at channel speeds of 40 Gbit/s and above [5, 7, 8], and OOK is the (at least traditionally) most common modulation format.

The practical consequences of intrachannel nonlinear effects is that the signal pulses can attract or repel each other and energy can be transferred either from the signal pulses to empty bit slots or between different signal pulses. These effects are referred to as *timing jitter*, generation of *ghost pulses*, and *amplitude jitter*, respectively. The fact that the Kerr nonlinearity can give rise to timing jitter in, e.g., soliton communication systems is well known [3], but reports and analyses of amplitude jitter and ghost pulses in dispersion-managed systems are of considerably later date [9–11]. The present thesis describes these phenomena analytically and numerically, shows their practical implications and discusses possible countermeasures.

The thesis is organised as follows: Chapter 2 gives a brief introduction to the model used to describe light propagating in an optical fibre. In Chapter 3, timing jitter is discussed and the main features of Paper A are summarised. In Chapter 4, a perturbation analysis is presented, which provides a way of calculating the nonlinear effects. This is also the topic of Paper B. Chapter 5 uses the analytical results to explain numerical simulations. The obtained results provide information about the range (measured in bit slots) of the nonlinear interaction and show how the nonlinear distortion increases its strength during propagation. This is reported in Paper C. In Chapter 6, a number of techniques for suppressing the nonlinear distortion are described with special emphasis given to the effects of phase shifting of the signal pulses, which has been considered in Papers D and E. Finally, two types of all-optical regenerators are discussed in Chapter 7 providing an introduction to Papers F and G.

Chapter 2

Modelling optical transmission

The propagation of light in an optical fibre is modelled by the *nonlinear Schrödinger equation* (NLSE) [3], which is an accurate model equation for several phenomena of fundamental importance. The NLSE is presented below and a short introduction to the different physical processes it models is given. An overview of the fundamental methods for compensation of signal degradation, fibre amplifiers and dispersion management, is also provided.

2.1 The nonlinear Schrödinger equation

The NLSE is formulated in terms of the envelope of the electric field, $\psi(z,t)$, which is assumed to vary slowly compared to the carrier wave. Depending on which processes one wishes to model, different terms have to be included. Here the equation

$$i\frac{\partial\psi}{\partial z} = \underbrace{\frac{\beta_2}{2}\frac{\partial^2\psi}{\partial t^2} + i\frac{\beta_3}{6}\frac{\partial^3\psi}{\partial t^3}}_{\text{dispersion}} - \underbrace{i\frac{\alpha}{2}\psi}_{\text{atten.}} - \underbrace{\gamma|\psi|^2\psi}_{\text{nonlin.}} \tag{2.1}$$

will be discussed. The terms have been labelled with their corresponding physical effects, which are now discussed individually.

2.1.1 Chromatic dispersion

The dispersive properties of the optical fibre, which are described by the dispersion relation, give rise to the dispersion terms in Eq. (2.1). Taylor expansion of the dispersion relation around the carrier frequency ω_0 yields

$$\beta(\omega) = \beta_0 + \beta_1(\omega - \omega_0) + \frac{\beta_2}{2}(\omega - \omega_0)^2 + \frac{\beta_3}{6}(\omega - \omega_0)^3 + \ldots, \quad (2.2)$$

where β is the wave number and

$$\beta_i \equiv \left.\frac{d^i\beta}{d\omega^i}\right|_{\omega=\omega_0}. \quad (2.3)$$

The wave number of the carrier wave is β_0. There is no corresponding term in the NLSE since this corresponds to the fast carrier wave phase variation, $\exp[i(\beta_0 z - \omega_0 t)]$, which is not present in the slowly varying envelope ψ.

The term involving β_1 gives rise to the group velocity of the envelope, $v_g = 1/\beta_1$, and it has been removed from Eq. (2.1) by a substitution of variables that describes the pulse in a reference frame moving with the group velocity. The new variable, here denoted by t, is referred to as *retarded time*.

The term proportional to β_2, the *group-velocity dispersion parameter* (GVD parameter), makes a propagating envelope broader in time according to the asymptotic expression [2]

$$\Delta t = L\beta_2\Delta\omega \equiv LD\Delta\lambda, \quad (2.4)$$

where L is the propagation distance, $\Delta\omega$ is the bandwidth of the signal, and $\Delta\lambda$ is the corresponding wavelength range. Equation (2.4) implicitly defines D, called the *dispersion parameter*, by giving the asymptotic relation between Δt, L, and $\Delta\lambda$. The relation between the GVD parameter and the dispersion parameter is

$$D = -\frac{2\pi c}{\lambda^2}\beta_2, \quad (2.5)$$

where λ is the wavelength and c is the speed of light.

The GVD introduces a characteristic length scale called the *dispersion length*. This can be understood as the distance the pulse must

propagate to be considerably affected by the GVD. The definition is given by

$$L_D \equiv \frac{t_0^2}{|\beta_2|}, \tag{2.6}$$

where t_0 is the $1/e$-width of the pulse. With $D = 16$ ps/(nm×km) and $t_0 = 5$ ps (corresponding to 8.3 ps full width at half maximum (FWHM)), which are typical values for a 40 Gbit/s system, the value of L_D is approximately 1.2 km. This is much shorter than the typical fibre length.

The term proportional to β_3 gives rise to TOD. This is normally a much weaker effect than the GVD, but it becomes the main dispersive effect if the fibre is operated at a wavelength where $D = 0$ or if the GVD is (perfectly) compensated for by using a dispersion management technique. In the present work the impact of TOD will not be taken into consideration.

It is possible to include more terms into the Taylor expansion above, but at a channel speed of 40 Gbit/s the inclusion of GVD and TOD leads to sufficient accuracy.

2.1.2 Attenuation

Although communication fibres are extremely transparent, the fibre attenuation eventually gives rise to significant power loss during propagation. An SMF has a power attenuation of 0.2 dB/km, which implies that a typical fibre amplifier power gain of 20 dB is sufficient for a propagation distance of approximately 100 km. The attenuation α has the dimension m^{-1}, and a characteristic attenuation length can be defined according to

$$L_A \equiv \frac{1}{\alpha} \approx 22 \text{ km}. \tag{2.7}$$

2.1.3 Kerr nonlinearity

The nonlinear Kerr effect in Eq. (2.1) is due to the power dependence of the refractive index, which in turn affects the dispersion relation

$$\tilde{\beta}(\omega, P) \equiv \beta(\omega) + \gamma P = \beta(\omega) + \gamma|\psi|^2, \tag{2.8}$$

where P is the wave power. (The envelope is normalised to make $|\psi|^2$ equal to the power.) The constant γ, called the *nonlinear parameter*,

depends on the type of fibre used. This modification of the dispersion relation introduces the nonlinear term in the NLSE.

The Kerr term gives rise to *self-phase modulation* (SPM) and makes *soliton pulses* possible, which propagate without changing the shape. The balance between CD and Kerr nonlinearity in such a pulse can be understood qualitatively by comparing Eq. (2.1) with the Schrödinger equation from quantum mechanics, which in one dimension reads

$$i\hbar\frac{\partial\psi}{\partial t} = -\frac{\hbar^2}{2m}\frac{\partial^2\psi}{\partial x^2} + V(x)\psi. \tag{2.9}$$

By removing attenuation and TOD from Eq. (2.1) and assuming that $\beta_2 < 0$ there is a direct correspondence between the terms of the two differential equations. The potential term for a pulse is directly identified as

$$V(t) = -\gamma|\psi|^2. \tag{2.10}$$

Thus, the pulse arranges a potential well for itself and the soliton is a bound state existing in this self-organised well.

Apparently, the soliton is the ideal optical information carrier, and this impression is further strengthened by the fact that it is also very stable against perturbations. This has lead to the rapid development of *soliton communication systems* during the 1990s, but these systems suffer from a number of shortcomings connected to the nonlinear process that makes the solitons possible [2]. One of these is loss-induced soliton broadening. Since the nonlinear compressive effects depends on the pulse power, a loss of power leads to a need for pulse shape adjustment. The pulse will then increase its width in order to make the dispersive broadening effects weaker, and this will eventually lead to overlap between neighbouring signal pulses. Another effect is soliton interaction. In a train of pulses the effect of *cross-phase modulation* (XPM) will, similar to SPM above, act as a potential term, which, via the CD, makes the pulses attract or repel each other. This gives rise to random pulse location shifts, known as *timing jitter*, which eventually makes the bit train impossible to decode.

In current transmission systems the signal pulses are designed to propagate linearly and the Kerr nonlinear effects are typically unwanted. The strength of the nonlinearity can be characterised by the *nonlinear length*, defined as

$$L_{NL} \equiv \frac{1}{\gamma P_0}, \tag{2.11}$$

where P_0 is the initial pulse power. Typical values for a 40 Gbit/s channel are $P_0 = 10$ mW and $\gamma = 2$ W^{-1}km^{-1}, which gives $L_{NL} = 50$ km, showing that $L_{NL} \gg L_D$. This regime of weak nonlinear effects, which is the focus of this thesis, is often referred to as the *pseudolinear regime*, since the linear effects dominate the pulse dynamics [1]. However, the nonlinear effects will distort the signal to a certain amount, giving rise to timing jitter, amplitude jitter, and ghost pulses, and these effects are thoroughly discussed in Chapters 3 and 4.

2.2 The linear Schrödinger equation

The NLSE will be investigated analytically by assuming that the nonlinear Kerr effect is a small perturbation. Thus, the solution to the linear Schrödinger equation, which is obtained by setting $\gamma = 0$ in Eq. (2.1), will act as the unperturbed solution. If the TOD term is discarded, the linear Schrödinger equation becomes

$$i\frac{\partial \psi}{\partial z} = \frac{\beta_2}{2}\frac{\partial^2 \psi}{\partial t^2} - i\frac{\alpha}{2}\psi. \tag{2.12}$$

As mentioned in Chapter 1 the considered modulation format is RZ, and the initial pulses are modelled as unchirped Gaussian pulses,

$$\psi(0,t) = A_0 \exp\left[-\frac{(t-\bar{t})^2}{2t_0^2}\right]. \tag{2.13}$$

The solution to Eq. (2.12) is then

$$\psi(z,t) = \frac{\sqrt{p(z)}A_0}{\sqrt{1-iB(z)}} \exp\left[-\frac{(t-\bar{t})^2}{2t_0^2[1-iB(z)]}\right], \tag{2.14}$$

where $B(z)$ is the accumulated dispersion, here defined in dimensionless form according to

$$B(z) \equiv \frac{1}{t_0^2}\int_0^z \beta_2(z')\,dz', \tag{2.15}$$

and the attenuation factor, $p(z)$, is defined as $p(z) \equiv P(z)/P_0$, where P_0 is the initial pulse power and $P(z)$ is the local value. In a fibre with constant attenuation $p(z)$ is proportional to $e^{-\alpha z}$ between amplifiers, making the pulse power decay exponentially during propagation.

2.3 Compensation of linear signal degradation

In order to cancel the effects of attenuation and dispersion the signal has to be amplified and the dispersive broadening needs to be compensated for. This can be done with fibre amplifiers and dispersion management.

2.3.1 Fibre amplifiers

The amplification of the signal pulses is done either by using lumped (optical) amplifiers or by using distributed Raman amplification. The amplifiers and pumping schemes are complicated, and introduce considerable complexity into the system. A good example is the noise generation, which is an inherent part of any amplifier. This is a major effect that degrades the OSNR and must be accounted for in system simulations. In order to describe the amplification it is then necessary to, e.g., model the noise characteristics and the frequency dependence of the gain accurately. The purpose of the present thesis is to provide understanding for the Kerr nonlinear processes, and in order to focus on these effects the system is simplified by using ideal amplifiers, which merely multiply the signal by a gain factor. This will restore the power level and increase the strength of the nonlinear interaction.

2.3.2 Dispersion management

The dispersion compensation can be performed in different ways, but only the use of DCF will be considered here. In such a fibre the GVD parameter has opposite sign as compared to an SMF, and the technique uses the fact that the total accumulated dispersion, $B(L)$, after propagation through the system of length L is equal to

$$B(L) = \frac{1}{t_0^2} \int_0^L \beta_2(z')\, dz'. \tag{2.16}$$

By selecting the DCF fibre lengths appropriately this integral can be made zero, i.e., perfect GVD compensation can be achieved.

Figure 2.1 shows an arrangement of two *dispersion-managed cells* (DM cells). In typical real fibres $|D_{\mathrm{DCF}}| \approx 5|D_{\mathrm{SMF}}|$, but in Fig. 2.1 it has been assumed that $|D_{\mathrm{SMF}}| = |D_{\mathrm{DCF}}|$. (This is also chosen in some numerical simulations in this thesis). Using this assumption the length of each fibre, except possibly the first and last, is L, which means that one DM cell is $2L$ long. The figure defines the launch position, X,

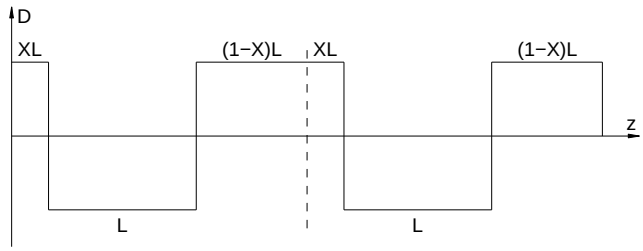

Figure 2.1: A system with two DM cells and launch position X.

from the fact that the length of the SMF at the start of the system is XL. The remaining part of that fibre, $(1-X)L$, is placed at the end of the system. In this way suitable precompensation of the pulses can be obtained, which, as will be shown, is an important method to suppress timing jitter.

One of the most expensive steps in setting up a fibre communication link is to install the fibre, and therefore there are economical reasons to use already installed SMF. In order to use dispersion management, the DCF is placed at suitable locations along or at the ends of the fibre link. Thus the launch position is easy to choose and can be used to optimise the properties of the communication system.

2.4 Measuring the signal distortion

The aim of an optical communication system is to transmit digital data correctly, which in a practical context means that the bit-error rate (BER) should be lower than a given limit. A commonly used criterion is that among 10^9 bits at most one bit may on average be incorrectly transmitted, which corresponds to a BER $< 10^{-9}$. However, to do a direct numerical simulation of the BER would in principle demand that a bit train that is significantly longer than 10^9 pulses is used, and this requires extreme computational efforts. Instead a shorter pulse train is simulated and a statistical approach is used to predict the BER.

If the statistics of the signal distortion can be assumed to be Gaussian, a signal quality measure known as the Q-value can be related to the BER. The definition is

$$Q \equiv \frac{I_1 - I_0}{\sigma_1 + \sigma_0}, \tag{2.17}$$

where I_1 (I_0) and σ_1 (σ_0) are the mean optical power level (or electric current level in the receiver) and the standard deviation of the ones (zeroes) due to noise, respectively. When the decision threshold is optimised the BER corresponding to a given Q-value is [2]

$$\mathrm{BER} = \frac{1}{2}\,\mathrm{erfc}\left(\frac{Q}{\sqrt{2}}\right) \approx \frac{\exp(-Q^2/2)}{Q\sqrt{2\pi}}. \tag{2.18}$$

The mentioned assumption of Gaussian noise statistics is quite important. If, e.g., all-optical regeneration (see Chapter 7) is carried out the noise statistics can be changed significantly, and BER predictions using the Q-value should then be avoided. It should also be noticed that the Q-value is only suitable for OOK data, and it should not be used, e.g., when the data is encoded into the phase of the optical signal.

The *sensitivity* of an optical receiver is the minimum average received power required to reach the target BER. An alternative measure of the amount of signal distortion is the degradation of sensitivity, since the introduction of noise must be compensated by an increased power in order to obtain a sufficiently high OSNR. The necessary power increase is then referred to as a *power penalty*. In the current context, where the main interest is the nonlinear signal distortion, this is not a suitable measure since an increase power level can lead to further system performance degradation.

Chapter 3

XPM-induced signal distortion

It is well known that the Kerr nonlinearity gives rise to attraction and repulsion between pulses [3]. In fact, this is one of the major problems in soliton communication systems, since the pulses drift away randomly instead of staying in their assigned bit slots. This will decrease the pulse power in the middle of the bit slot where the field is sampled and eventually the pulse train will be impossible to decode.

In the present thesis the nonlinear effects are assumed to be weak and they cannot balance the dispersive effect, leading to a need for dispersion management. The basic effect, that the pulses will attract or repel each other, is however still present and of importance. This is known as (intrachannel) *timing jitter*.

Paper A presents results describing how two pulses interact during propagation through a dispersion-managed system. The analysis is based on a variational approach, which assumes that the pulses remain Gaussian-shaped (as predicted by Eq. (2.14)). A similar, independently conducted analysis is found in Ref. [12]. Paper A reports the suppressive effects that can be obtained by proper precompensation by optimising the launch position. Ref. [12] emphasises the increase in the collapse distance that can be obtained by proper placement of the amplifier, but this does not generalise to long pulse trains. It should be noticed that both these publications consider interaction in a pulse train consisting of only two signal pulses. In a realistic pulse train there is interaction between many pulses and this changes the results considerably. This will be further clarified in Chapter 5.

Additional results using the equations from Ref. [12] are found in Ref. [13], but the pulse train length is very limited also in this case. Further theoretical treatments of the subject are found in Refs. [14–16]. Of special interest is the importance of precompensation [14] and the results valid for longer pulse trains [15].

3.1 Governing equations

In order to describe how two pulses affect each other the NLSE

$$i\frac{\partial\psi}{\partial z} = \frac{\beta_2}{2}\frac{\partial^2\psi}{\partial t^2} - i\frac{\alpha}{2}\psi - \gamma|\psi|^2\psi \tag{3.1}$$

is rewritten by introducing $\psi = \psi_1 + \psi_2$. The nonlinear term then becomes

$$|\psi|^2\psi = |\psi_1|^2\psi_1 + |\psi_2|^2\psi_2 + 2|\psi_1|^2\psi_2 + 2|\psi_2|^2\psi_1 + \psi_1^2\psi_2^* + \psi_2^2\psi_1^*. \tag{3.2}$$

In order to analyse the timing jitter, Eq. (3.1) must be decomposed into two equations separately describing ψ_1 and ψ_2, respectively. To do this, the two terms $\psi_1^2\psi_2^*$ and $\psi_2^2\psi_1^*$ should be discarded, since the XPM-induced pulse interaction in a pseudolinear system, where $L_{NL} \gg L_D$, is an incoherent process. The discarded terms instead give rise to ghost pulses in the empty neighbouring bit slots, and their role will be made clear in Chapter 4, where all terms of Eq. (3.2) are taken into consideration. The coupled system to be used for describing the two-pulse timing jitter interaction is then obtained as [3]

$$i\frac{\partial\psi_1}{\partial z} = \frac{\beta_2}{2}\frac{\partial^2\psi_1}{\partial t^2} - i\frac{\alpha}{2}\psi_1 - \gamma\left(|\psi_1|^2 + 2|\psi_2|^2\right)\psi_1, \tag{3.3}$$

$$i\frac{\partial\psi_2}{\partial z} = \frac{\beta_2}{2}\frac{\partial^2\psi_2}{\partial t^2} - i\frac{\alpha}{2}\psi_2 - \gamma\left(|\psi_2|^2 + 2|\psi_1|^2\right)\psi_2. \tag{3.4}$$

3.2 Physical interpretation

Eqs. (3.3) and (3.4) are similar to Eq. (3.1), since dispersion and attenuation affect the two separate pulses in the same way. The difference is that two new nonlinear XPM terms appear, and these give rise to a coupling between the two pulses. The nonlinear terms can be interpreted as potential terms acting on the pulses, and if $\beta_2 < 0$ the potential term for pulse ψ_2 can, in analogy with Section 2.1.3, directly be identified as

$$V(t) = -\gamma\left(|\psi_2|^2 + 2|\psi_1|^2\right). \tag{3.5}$$

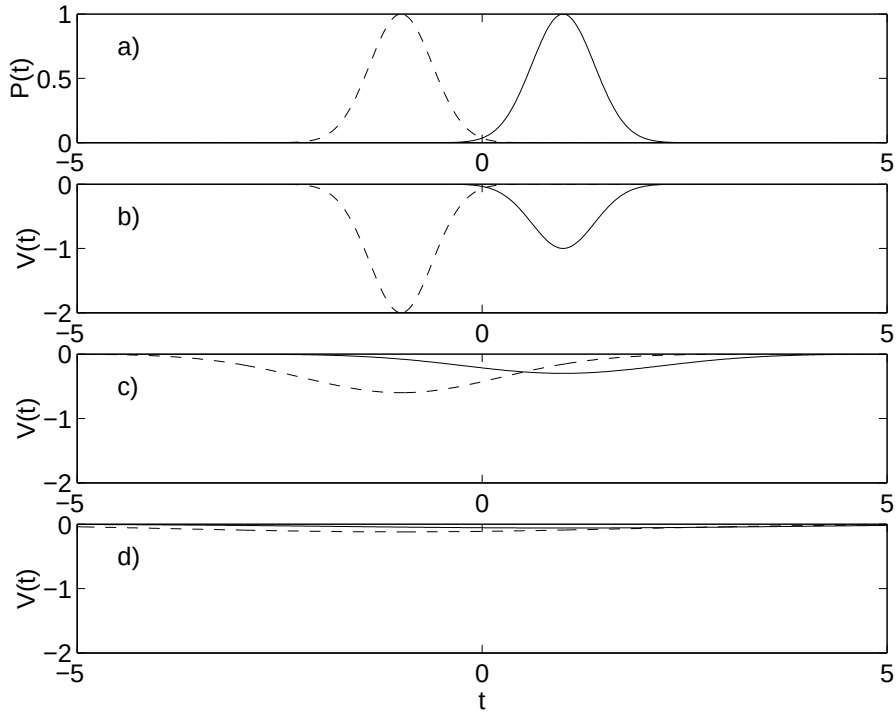

Figure 3.1: a) Two signal pulses. b)–d) The two potential terms for the right pulse when $z \ll L_D$, $z \sim L_D$, and $z \gg L_D$, respectively.

The first part (the SPM term) acts to keep the pulse together, and the second (the XPM term) introduces an asymmetry that will accelerate the pulse. Figure 3.1 can be taken as a starting point for a qualitative discussion of how the strength of the interaction changes during propagation. Figs. 3.1a and b show the initial pulse powers and the two potential terms affecting the pulse indicated by a solid line. The XPM is initially weak since the dashed curve is close to zero over the pulse, making the potential flat. In Fig. 3.1c the pulses have propagated a certain distance which has made them overlap partially. (The overlap can be defined as the pulse width divided by the pulse separation.) The right pulse will experience a force directed to the left, which will give rise to an acceleration. (Since the analogy to mechanics is helpful, the second derivative of the temporal position is referred to as "the acceleration", although the roles of space and time are interchanged.) The amount of broadening corresponds to a propagation distance approximately equal

to L_D. In Fig. 3.1d the pulses have propagated much longer than the dispersion length and the overlap is strong. However, the dashed curve is shallow and, since the force is the negative derivative of the potential, the acceleration is expected to be low.

In summary, in a strongly dispersion-managed system where the fibre length $L \gg L_D$, the pulses will initially not be affected by the presence of the other pulse. When the pulses are partially overlapping they are accelerated, but the force decreases its strength as the pulses become strongly overlapping, and they will then move with a constant new group velocity. These qualitative arguments can be used to interpret the results obtained in Paper A.

3.3 The timing jitter equations

The equations for the timing jitter in Paper A were obtained using variational analysis and the Ritz optimisation method, which selects the best approximation to the exact solution of a differential equation within a given set of trial functions [17]. Since the nonlinear effects are weak it is reasonable to view the two signal pulses as slightly perturbed, linearly propagating pulses. Thus the trial functions were chosen to be Gaussian pulses propagating according to the linear Schrödinger equation but having perturbed temporal positions and widths. By reformulating the coupled equations as a variational problem it is a straight-forward task to find the differential equations as is done in Paper A. When treating these equations it is assumed that the width is not changed by the nonlinear effects, and it can then be found from the linear propagation equation. This yields the main equation in Paper A.

Instead of discussing the details of the variational analysis an alternative derivation is presented here for the unattenuated case, which provides good insight into the physics of the problem. It is assumed that the two pulses are denoted by ψ_1 and ψ_2. The mean temporal position of ψ_2 is defined as

$$\langle t \rangle = \frac{\int_{-\infty}^{\infty} t|\psi_2|^2\,dt}{\int_{-\infty}^{\infty} |\psi_2|^2\,dt} = \frac{1}{W}\int_{-\infty}^{\infty} t|\psi_2|^2\,dt, \tag{3.6}$$

where W is the pulse energy, which is a conserved quantity when the attenuation is neglected. Taking the derivative of this expression with respect to z, using Eq. (3.4) to replace the z-derivatives of ψ_2, and by

using partial integration, we obtain

$$\frac{d^2\langle t\rangle}{dz^2} = -i\frac{\beta_2}{W}\int_{-\infty}^{\infty}\left(\frac{\partial\psi_2}{\partial z}\frac{\partial\psi_2^*}{\partial t} - \frac{\partial\psi_2}{\partial t}\frac{\partial\psi_2^*}{\partial z}\right)dt. \tag{3.7}$$

Using again Eq. (3.4) to replace the z-derivatives, the resulting equation is found to be

$$\frac{d^2\langle t\rangle}{dz^2} = -\frac{2\gamma\beta_2}{W}\int_{-\infty}^{\infty}|\psi_2|^2\frac{\partial}{\partial t}|\psi_1|^2\,dt. \tag{3.8}$$

This can be directly interpreted by using the analogy with mechanics. The left hand side of the equation is the acceleration (the roles of time and space are interchanged). The force is equal to the negative gradient of the potential, i.e.,

$$F = -\frac{\partial V}{\partial t} = -\frac{\partial}{\partial t}\left(-2\gamma|\psi_1|^2\right) = 2\gamma\frac{\partial}{\partial t}|\psi_1|^2, \tag{3.9}$$

and the mean force acting on ψ_2 is

$$\langle F\rangle = \frac{\int_{-\infty}^{\infty}F|\psi_2|^2\,dt}{\int_{-\infty}^{\infty}|\psi_2|^2\,dt} = \frac{2\gamma}{W}\int_{-\infty}^{\infty}|\psi_2|^2\frac{\partial}{\partial t}|\psi_1|^2\,dt. \tag{3.10}$$

The GVD parameter relates this force to the acceleration in Eq. (3.8), giving the general result for the timing jitter. It should be noticed that by changing the sign of β_2 both the velocity and the acceleration will change signs. The fact that the velocity makes a finite jump indicates that the analogy to mechanics is not complete.

In order to examine the specific case of two propagating Gaussian pulses expression (2.14) is used, with the temporal positions of ψ_1 and ψ_2 set to $\mp\langle t\rangle$, respectively. By simplifying we get the expression

$$\frac{d^2\langle t\rangle}{dz^2} = \mathrm{sign}(\beta_2)\frac{2\sqrt{2}}{L_{NL}L_D}\frac{\langle t\rangle}{(1+z^2/L_D^2)^{3/2}}\exp\left[-\frac{2\langle t\rangle^2}{a_0^2(1+z^2/L_D^2)}\right]. \tag{3.11}$$

Equation (3) from Paper A, can be recovered by using $\Delta t = 2\langle t\rangle$, $W = \sqrt{\pi}a_0A_0^2$ and the definitions for L_D and L_{NL}. The right hand side expression initially has a very small value but it increases and reaches a maximum when z is increased, and then it falls off slowly. It has been plotted qualitatively in, e.g., Ref. [11].

3.4 Timing jitter simulations

A numerical simulation of the timing jitter for pulse ψ_2 in a system consisting of two fibres (an SMF followed by a DCF, corresponding to launch position $X = 1$, see Fig. 2.1) is shown in Fig. 3.2. The fibers are 50 km long and the dispersion parameters are ± 10 ps/(nm×km). The bit slot is 25 ps (corresponding to 40 Gbit/s) and the pulse width is 5 ps FWHM. The nonlinear parameter is $\gamma = 2$ W^{-1}km^{-1}, the pulse energy is 50 fJ, and the attenuation has been neglected.

To understand the simulated result it should be remembered that the second derivative of $\langle t \rangle$ is large only where the pulses are partially overlapping. Otherwise it is close to zero. The first region of strong interaction, i.e., partial pulse overlap occurs when $z \sim 3$ km, and the acceleration in this region changes the velocity from zero to a constant value. Pulse ψ_2 is shifted toward earlier times, and this means that the pulses attract each other in the first fibre. When the pulses enter the second fibre the temporal position is continuous, but the velocity changes its sign. The velocity of the pulse is directly related to the frequency shift by the dispersion parameter according to

$$\frac{d\langle t \rangle}{dz} = -2\pi\beta_2 \, \Delta f, \tag{3.12}$$

and the frequency shift, which is continuous, is studied in Paper A. Close to the end of the system the pulses are again partially overlapping and the acceleration is significant. It should be noticed that the frequency shift and the modulus of the velocity are monotonous. This gives rise to an asymmetry and makes the final temporal position larger than the initial one. This is the timing jitter effect.

By using a different launch position the asymmetry can be counteracted. In Fig. 3.3 a simulation with $X = 1/2$ is shown. It is immediately seen that the final temporal position is very close to the initial one, which means that the timing jitter is strongly suppressed. Thus it is important to tune the precompensation in order to counteract the timing jitter.

However, $X = 1/2$ does not give exactly zero timing jitter. By testing different launch positions it is found that exact cancellation is obtained with a launch position close to, but not equal to $X = 1/2$. The reason is that the pulse separation is slightly larger after 50 km and this makes the interaction somewhat weaker in the second half of the system.

When the attenuation is included, the pulse dynamics are more complicated, and in particular the cancellation effect from precompensation

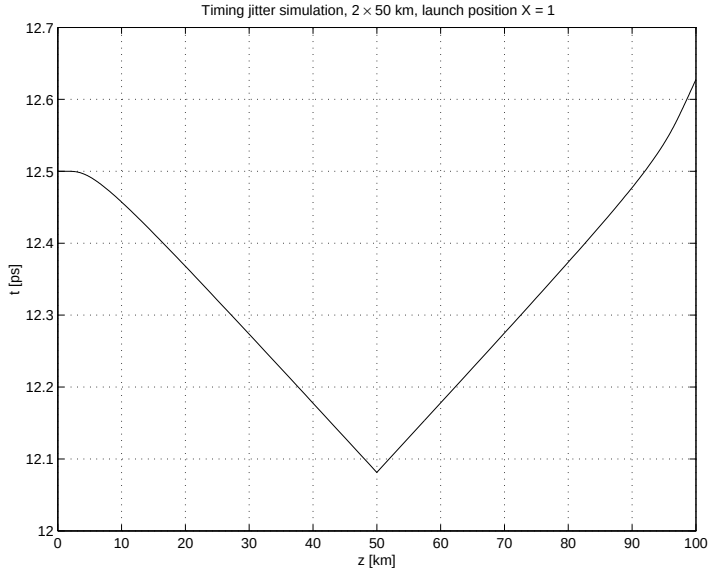

Figure 3.2: The temporal position of pulse A_2 as a function of propagation distance. Launch position $X = 1$.

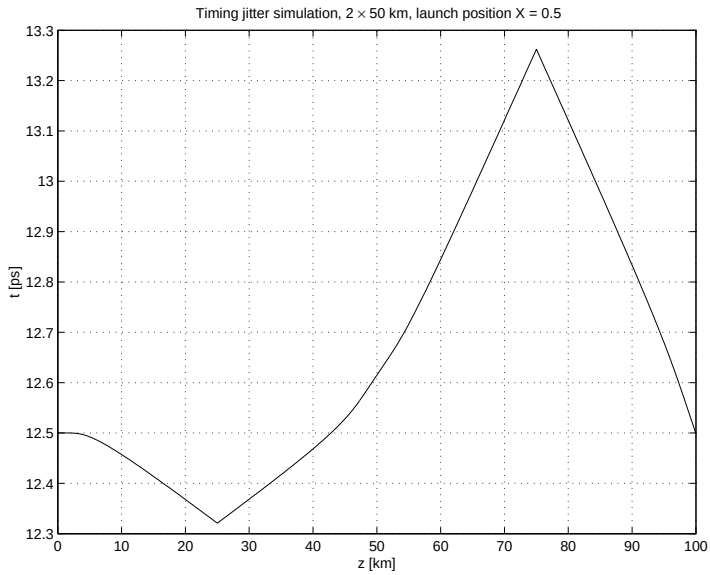

Figure 3.3: The temporal position of pulse A_2 as a function of propagation distance. Launch position $X = 1/2$.

of the signal is changed. This is due to the fact that the nonlinear interaction is power dependent, which leads to a need for adjustment of the precompensation when the power distribution in the system is changed. It is found in Paper A that cancellation of the timing jitter is still possible but it does not occur for a launch position close to 1/2. Similar suppressive effects from using proper precompensation have been reported several times [14, 18–21].

It has been suggested that the effect of timing jitter can be made low by making the power low in the regions of strong pulse interaction [22]. However, in a long pulse train the interaction strength is similar at all values of the accumulated dispersion, and it is not possible to suppress the timing jitter by designing the power distribution. This is discussed in more detail in Chapter 5.

3.5 Comment on amplitude shifting

The attraction or repulsion between pulses is one of the major obstacles in soliton communication systems, leading to bit errors due to timing jitter. It is known that by making the amplitudes of the soliton pulses unequal the interaction will be weaker [3]. At first sight it seems that this should be true also in pseudolinear systems. However, the effect from amplitude shifting in soliton systems is only indirect. By shifting the amplitude, the wavenumber of the pulse is modified, which changes the phase difference between the two pulses during propagation. For soliton pulses the sign of the interaction force depends on the phase difference, and the pulses will alternate between attracting and repulsing each other, which accounts for the effect. In the pseudolinear case no such effect is present, and shifting of the amplitudes is of no consequence.

Chapter 4

Perturbation analysis

A perturbation analysis of the NLSE is now presented. Ghost pulse generation, amplitude jitter, and timing jitter are all possible to describe using the obtained results and the goal is to understand how the nonlinear distortion is generated and how it can be counteracted. The current Chapter presents the analytical results and Chapter 5 contains a system study which is based on numerical simulations.

Additional descriptions of this topic can be found in the literature. In particular, the perturbation approach developed here has also been the starting point for two other research groups working independently on the problem [14–16,23–25]. Ref. [15] presents a perturbation analysis and describes ghost pulse generation and timing jitter. These results are extended in Ref. [14], where precompensation is studied, and Ref. [23], where the nonlinear effects are calculated by averaging over a long pulse train. Ref. [24] presents a mathematical treatment of a similar perturbation equation. The final temporal location of the perturbation is found, and it is emphasised that the ghost pulse energy grows in proportion to z^2 in a periodic system (i.e., the amplitude increases linearly). Furthermore, it is found that many signal pulses participate in the generation of a ghost pulse. Refs. [16] and [25] specialise in timing jitter and energy transfer, respectively, and suggests the use of distributed Raman amplification to decrease the nonlinear distortion. An alternative description, that is more similar to traditional FWM, is found in Ref. [26]. The interaction between three pulses is studied, and it is suggested that unequal pulse separation can suppress the nonlinear distortion. Longer pulse trains are considered in Ref. [13], where the nonlinear perturbation is found by summing over all possible triplets of signal pulses numerically.

4.1 The perturbation approach

Neglecting third order dispersion, the NLSE is

$$i\frac{\partial\psi}{\partial z} = \frac{\beta_2}{2}\frac{\partial^2\psi}{\partial t^2} - i\frac{\alpha}{2}\psi - \gamma|\psi|^2\psi. \tag{4.1}$$

This equation is analysed using the fact that the nonlinear effects are weak in the pseudolinear regime. Thus, we set $\psi = \psi_s + \psi_p$, where ψ_s is the signal pulse train propagating according to the linear equation obtained by setting $\gamma = 0$ in Eq. (4.1), and ψ_p is the perturbation generated by the nonlinearity. The pulses are assumed to be Gaussian shaped, which means that ψ_s is known exactly (see Section 2.2). Inserting $\psi = \psi_s + \psi_p$ into Eq. (4.1) gives

$$\begin{aligned} i\frac{\partial}{\partial z}(\psi_s+\psi_p) = \frac{\beta_2}{2}\frac{\partial^2}{\partial t^2}(\psi_s+\psi_p) - i\frac{\alpha}{2}(\psi_s+\psi_p) \\ -\gamma\Big(\underbrace{|\psi_s|^2\psi_s}_{O(1)}\underbrace{+2|\psi_s|^2\psi_p + \psi_s^2\psi_p^*}_{O(\psi_p)} \\ \underbrace{+2\psi_s|\psi_p|^2 + \psi_s^*\psi_p^2}_{O(\psi_p^2)}\underbrace{+|\psi_p|^2\psi_p}_{O(\psi_p^3)}\Big). \end{aligned} \tag{4.2}$$

Since $|\psi_p|$ is much smaller than $|\psi_s|$ all source terms except the dominant one can be neglected, which is the main approximation of the perturbation analysis. The fact that ψ_s solves Eq. (2.12) implies that the above equation can be split into the equation system

$$i\frac{\partial\psi_s}{\partial z} - \frac{\beta_2}{2}\frac{\partial^2\psi_s}{\partial t^2} + i\frac{\alpha}{2}\psi_s = 0, \tag{4.3}$$

$$i\frac{\partial\psi_p}{\partial z} - \frac{\beta_2}{2}\frac{\partial^2\psi_p}{\partial t^2} + i\frac{\alpha}{2}\psi_p = -\gamma|\psi_s|^2\psi_s. \tag{4.4}$$

4.1.1 Source terms from a pulse train

The optical signal consists of a number of data pulses,

$$\psi_s(z=0,t) = \sum_n \sigma_n\psi_n(z=0,t) = \sum_n \sigma_n\psi_0(z=0,t-nT_B), \tag{4.5}$$

where T_B is the bit slot, $\psi_0(z=0,t) = A_0\exp[-t^2/(2t_0^2)]$, and σ_n is equal to zero or one depending on whether bit slot n contains a signal

pulse or not. By inserting $\psi_s(z,t)$, which is the solution to Eq. (4.3) using $\psi_s(z=0,t)$ as initial condition, into the source term in Eq. (4.4) terms of the type $\psi_k\psi_l\psi_m^*$ are obtained. Although the source term is very complicated, the linearity of Eq. (4.4) asserts that the total ψ_p can be viewed as the sum of different contributions to the total perturbation given by the individual source terms. This means that the different nonlinear effects can be analysed individually by choosing the appropriate source term, which in the general case can be written $-\gamma\psi_k\psi_l\psi_m^*$.

The simple case of only two signal pulses, $\psi_s = \psi_1 + \psi_2$, serves well as a fundamental example. Inserting this expression into Eq. (4.4) the expanded source term becomes

$$-\gamma\left(|\psi_1|^2\psi_1 + |\psi_2|^2\psi_2 + 2|\psi_1|^2\psi_2 + 2|\psi_2|^2\psi_1 + \psi_1^2\psi_2^* + \psi_2^2\psi_1^*\right). \quad (4.6)$$

The first two terms of (4.6) give rise to SPM of the two signal pulses. The following two terms are the XPM terms, which will cause timing jitter. The last terms generate the ghost pulses by a transfer of energy from the signal pulses to the neighbouring empty bit slots. To visualise the effects of the different source terms, a numerical simulation for a single DM cell has been done. The two signal pulses are located at $t = 25$ ps and $t = 50$ ps, respectively and the different contributions from the source terms have been plotted in Fig. 4.1. To see, e.g., the SPM effect we must add $\psi = \psi_s + \psi_p$ and then plot $|\psi|^2$, but the point of Fig. 4.1 is only to show the relative strengths and the temporal positions of the different nonlinear effects. The ghost pulses are located close to $t = 0$ ps and $t = 75$ ps, respectively.

In the case of a general pulse train there are three different types of source terms, which now can be considered separately. Terms of the type $|\psi_k|^2\psi_k$ cause SPM, which lead to a slight change of the pulse width and amplitude. Terms of the type $|\psi_l|^2\psi_k$, $k \neq l$, are intrachannel XPM terms and cause timing jitter, see Chapter 3. Finally, terms of the types $\psi_k^2\psi_l^*$, $k \neq l$, and $\psi_k\psi_l\psi_m^*$, where k, l, and m are all different, cause intrachannel four-wave mixing (FWM), which gives rise to ghost pulses and amplitude jitter, respectively, depending on whether there is a signal pulse in the bit slot where the perturbation is generated.

4.2 The solution to the perturbation equation

The part of the total perturbation caused by the source term $S_{klm} \equiv -\gamma\psi_k\psi_l\psi_m^*$ is now calculated, and in the following this will be referred to

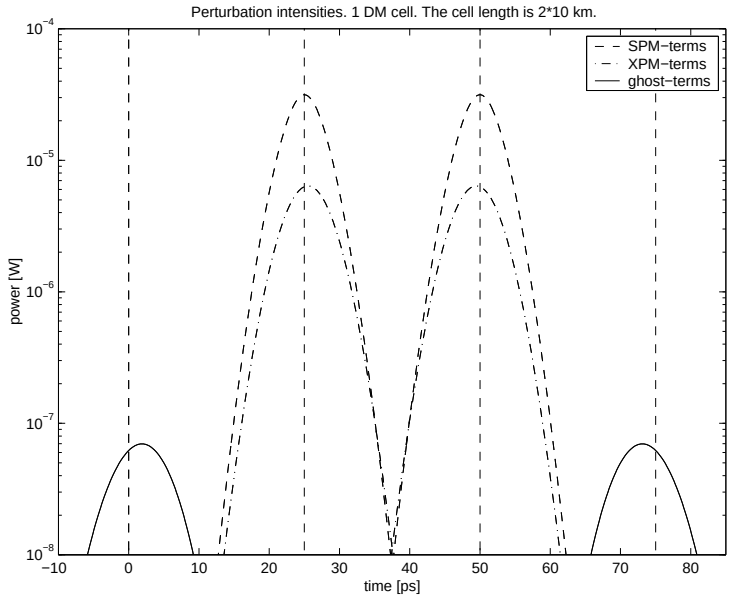

Figure 4.1: The resulting contributions from each of the individual source terms of the right hand side of Eq. (4.6).

as the (k, l, m) contribution. The system is quite general at this stage; no assumptions of fibre parameters or amplifier locations are made. The equation for the contribution is

$$i\frac{\partial \psi_p}{\partial z} - \frac{\beta_2}{2}\frac{\partial^2 \psi_p}{\partial t^2} + i\frac{\alpha}{2}\psi_p = S_{klm}(z,t). \tag{4.7}$$

Setting $\psi_p(z,t) = \sqrt{p(z)}a(z,t)$ (see Section 2.2 for the definition of $p(z)$) gives

$$\frac{\partial a}{\partial z} + i\frac{\beta_2}{2}\frac{\partial^2 a}{\partial t^2} = -\frac{i}{\sqrt{p}}S_{klm}. \tag{4.8}$$

Fourier transformation of Eq. (4.8) yields a simple equation for the transform $\tilde{a}(z,\omega)$,

$$\frac{\partial \tilde{a}}{\partial z} - i\omega^2\frac{\beta_2}{2}\tilde{a} = -\frac{i}{\sqrt{p}}\tilde{S}_{klm}, \tag{4.9}$$

and the solution is obtained by multiplying (4.9) by $\exp(-i\omega^2 t_0^2 B/2)$ and integrating $\int_0^L \cdot\, dz$, i.e., over the entire system. It is assumed that the net dispersion in the system is zero, i.e., $B(L) = 0$ (see Eq. (2.15))

and that the losses are compensated for, i.e., $p(L) = 1$. Going back to $\tilde{\psi}_p$ and inverse Fourier transforming one obtains

$$\psi_p(L,t) = -i \int_0^L \frac{1}{\sqrt{p}} \mathcal{F}^{-1}\left[\mathcal{F}[S_{klm}] e^{-\frac{i}{2}\omega^2 t_0^2 B}\right] dz. \tag{4.10}$$

This is the general, exact solution of Eq. (4.7) for the (k,l,m) contribution after propagation of the signal pulses through a given system. By inserting the linearly propagating Gaussian pulses (given by Eq. (2.14)) the resulting expression becomes

$$\begin{aligned}
&\psi_p(L,t) = \\
&\quad iA_0^3 \int_0^L \frac{\gamma p}{\sqrt{1+2iB+3B^2}} \times \\
&\quad \exp\left\{-\frac{1}{2}\frac{3+iB}{1+3iB}\left[\tau^2 - 2\tau\frac{(1+iB)(\tau_k+\tau_l)+(1-iB)\tau_m}{3+iB}\right]\right\} \times \\
&\quad \exp\Bigg(-\frac{1}{2}\frac{1}{1+B^2}\Bigg\{(\tau_k^2+\tau_l^2)(1+iB)+\tau_m^2(1-iB) - \\
&\qquad\qquad [(\tau_k+\tau_l)(1+iB)+\tau_m(1-iB)]^2 \frac{iB}{1+3iB}\Bigg\}\Bigg) dz,
\end{aligned} \tag{4.11}$$

where the notation $\tau = t/t_0$, $\tau_k = t_k/t_0$ etc. has been used.

4.2.1 The temporal location of a contribution

It should be noticed that the temporal location of the integrand in Eq. (4.11) depends on the value of B. The integrand has been written as the product of three factors of which two are exponential functions and these have been arranged so that there is no time dependence in the second one. Therefore only the first exponential function needs to be studied here. It is seen that it is Gaussian-shaped, and by studying the polynomial in τ the temporal location can be deduced.

In the limit $|B| \ll 1$ the polynomial that determines the temporal location of the Gaussian pulse can be approximately determined from

$$\begin{aligned}
\tau^2 - 2\tau\frac{(1+iB)(\tau_k+\tau_l)+(1-iB)\tau_m}{3+iB} &\approx \tau^2 - 2\tau\frac{\tau_k+\tau_l+\tau_m}{3} \\
&= \left(\tau - \frac{\tau_k+\tau_l+\tau_m}{3}\right)^2 - \left(\frac{\tau_k+\tau_l+\tau_m}{3}\right)^2,
\end{aligned} \tag{4.12}$$

which shows that the location for the perturbation is $t = (t_k + t_l + t_m)/3$, i.e., the average temporal position between the generating signal

pulses. This seems to contradict the commonly accepted fact that the contribution is located at $t = t_k + t_l - t_m$. However, the amplitude of the generated perturbation is small when $|B| \ll 1$ due to the fact that there is no signal pulse overlap, and in a typical system the main part of the perturbation is generated in regions where $|B| > 1$. Thus, this prediction is not valid in such a system, and there is no contradiction.

The opposite limit, $B \gg 1$, gives the expected result. In this case the approximate polynomial is

$$\begin{aligned}\tau^2 - 2\tau\frac{(1+iB)(\tau_k+\tau_l)+(1-iB)\tau_m}{3+iB} &\approx \tau^2 - 2\tau\frac{iB(\tau_k+\tau_l)-iB\tau_m}{iB} \\ &= [\tau-(\tau_k+\tau_l-\tau_m)]^2 - (\tau_k+\tau_l-\tau_m)^2. \end{aligned} \tag{4.13}$$

It is seen that the perturbation is located at $t = t_k + t_l - t_m$, i.e., the contribution (k, l, m) ends up in bitslot number $k+l-m$. This has been reported several times, see, e.g., Ref. [24]. However, this points out one interesting feature; the temporal location of the perturbation depends on the length of the system. Generally, the source term, which is a product of three signal pulses, is temporally located between the pulses, but the generated perturbation is frequency shifted, which means that it will propagate with a different group velocity. This velocity shift makes the perturbation change its temporal position to its final value. This has been discussed in Paper B.

The fact that the perturbation is frequency shifted suggests that it might be removed by filtering. However, the shift is small compared to the bandwidth of the signal. This can be seen by using the equation

$$\frac{d\Delta T}{dz} = -2\pi\beta_2\Delta f, \tag{4.14}$$

which is considered in Paper A. In the second fibre of a DM cell the $(1, 1, 2)$ contribution will shift its temporal position from $t = 4T_B/3$ to $t = 0$. If the fibre length is $L = 100$ km and the dispersion parameter is $D = 16$ ps/(nm×km), the frequency shift is

$$|\Delta f| = \frac{4T_B/3}{2\pi|\beta_2|L} \approx 2.6 \text{ GHz}. \tag{4.15}$$

This shift is much smaller than the signal bandwidth, and it is clear that it is not possible to remove the nonlinear distortion by filtering.

Since the temporal positions are known, the contributions to the total perturbation in one chosen bit slot can be studied. Thus, by demanding that $k + l - m = 0$, the contributions will end up in bit slot

zero. The expression $m = k + l$ is therefore inserted into Eq. (4.11), and since the signal is sampled in the middle of the bit slot this particular point is studied by setting $t = 0$. The expression for the contribution then becomes

$$\psi_p(L,0) = iA_0^3 \int_0^L \frac{\gamma p}{\sqrt{1+2iB+3B^2}} \times \exp\left\{ -\frac{\nu^2}{2} \frac{1}{1-iB} \left[(k+l)^2 \frac{1-3iB}{1+3iB} + k^2 + l^2 \right] \right\} dz, \quad (4.16)$$

where $\nu \equiv T_B/t_0$. In a typical system $\nu \approx 5$. It should be remembered that γ, p, and B in Eq. (4.16) are all functions of z.

4.2.2 The perturbation from a periodic system

If a given system is periodic, i.e., consists of, e.g., a concatenation of a number of DM cells, the total perturbation is the number of cells times the perturbation after the first DM cell. This result follows directly from the fact that the integral (4.16) can be split into separate integrations over identical DM cells. This is discussed in Paper B.

The fact that the perturbation grows linearly with the number of DM cells is a considerable simplification when studying a system, and this result holds until the nonlinear perturbation is no longer small compared to the signal, i.e., until the basic assumption of the perturbation analysis is violated. This result is used in Chapter 5, where only a single DM cell is included in the system.

4.2.3 The role of attenuation

As seen from Eq. (4.16), the local pulse power acts as a weighting function on the source term. This has a number of consequences since the attenuation length is approximately 20 km, and real systems tend to be much longer than that. Thus, by neglecting the attenuation the nonlinear interaction will be overestimated in such an analysis. However, the unattenuated case can be used when discussing the dynamics of the interaction, and the effects of the attenuation can, due to its simple action, be considered at a later stage.

The power distribution is determined by the choice of amplifier locations, and this constitutes one of the major design considerations for a system. The particular choice made affects the amount of nonlinear interaction, but, as demonstrated in Chapter 5, the impact on ghost

pulses is not particularly strong. By changing the amplifier positions the amount of timing jitter changes, leading to a need to modify the precompensation.

The interaction range, i.e., the number of bit slots over which the nonlinear interaction is significant, is dependent on the amplifier positions. This is important when designing numerical system simulations, and in particular when choosing the length of the random bit train being considered. This is introduced in Chapter 5 and thoroughly discussed in Paper C.

4.2.4 The effect from precompensation

If a general launch position (see Section 2.3.2) is used, the pulses are precompensated and $B(z)$ will change its sign during propagation. As is seen from Eq. (4.16) changing the sign of $B(z)$ is equivalent to taking the complex conjugate of the integrand. Thus, the interaction in two parts of the system can add up to two times the real part of the integrand. It is known that symmetric precompensation can suppress both timing and amplitude jitter [14], and the reason is clearly seen in the case of amplitude jitter: When multiplying the real integral in Eq. (4.16) by an imaginary constant the result will be imaginary, which will cause the smallest possible amplitude change of the (real) signal pulse, i.e., it will give rise to the minimal amount of amplitude jitter.

The strong suppressive effect from using launch position $X \approx 1/2$ found in the timing jitter case is not seen for the power of the ghost pulses. This is shown in Chapter 5 when discussing Paper C.

The situation is more complicated when the effect of attenuation is included. The strength of the interaction is then weighted by the local power, which introduces an asymmetry and the case $X = 1/2$ will not make the contributions purely imaginary anymore. However, it has been found that by optimising the launch position, the timing jitter can still be efficiently suppressed [14, 18–21].

4.3 Approximate integration

The complicated expression (4.16) can be handled approximately, which allows more explicit results to be obtained. It will be found that the approximations introduce only small errors and that the final result makes it possible to draw several conclusions.

It order to prepare for the approximate analysis it is convenient to split the exponential function in the integrand of Eq. (4.16) according to $e^z = e^{\mathrm{Re}\, z} + e^{i\,\mathrm{Im}\, z}$, with the result

$$\psi_p(L,t) = iA_0^3 \int_0^L \frac{\gamma p}{\sqrt{1+2iB+3B^2}} \times \exp\left\{-\frac{\nu^2}{2}\frac{1}{1+B^2}\left[(k+l)^2\frac{1-3B^2}{1+9B^2}+k^2+l^2\right]\right\} \times \exp\left\{i\frac{\nu^2}{2}\frac{B}{1+B^2}\left[(k+l)^2\frac{5+9B^2}{1+9B^2}-(k^2+l^2)\right]\right\} dz. \quad (4.17)$$

4.3.1 Approximations

The integrand of Eq. (4.17) consists of a product of three factors, and the observation that the second factor is step-shaped allows significant simplifications. This is seen by examining the two limits $|B| \ll 1$ and $|B| \gg 1$. In the first case

$$\exp\left\{-\frac{\nu^2}{2}\frac{1}{1+B^2}\left[(k+l)^2\frac{1-3B^2}{1+9B^2}+k^2+l^2\right]\right\} \approx e^{-\nu^2(k^2+l^2+kl)}, \quad (4.18)$$

which is a very small number, and in the second case

$$\exp\left\{-\frac{\nu^2}{2}\frac{1}{B^2}\left[(k+l)^2\left(-\frac{1}{3}\right)+k^2+l^2\right]\right\} \approx e^{-\frac{\nu^2}{3B^2}(k^2+l^2-kl)}, \quad (4.19)$$

which rapidly approaches unity. A reasonable value for B at which the step is located is found by setting

$$\exp\left\{-\frac{\nu^2}{2}\frac{1}{1+B^2}\left[(k+l)^2\frac{1-3B^2}{1+9B^2}+k^2+l^2\right]\right\} = \exp(-1). \quad (4.20)$$

This quadratic equation for B^2 can be solved exactly, but the solution is somewhat complicated. A good approximation is instead obtained by assuming that $B \gg 1$, which implies that

$$\frac{1-3B^2}{1+9B^2} \approx -\frac{1}{3}. \quad (4.21)$$

This yields the result

$$B^2 = \frac{\nu^2}{3}(k^2+l^2-kl) - 1 \equiv B_{\mathrm{th}}^2. \quad (4.22)$$

Thus, the step-shaped function is approximated by unity in the regions where $B^2 > B_{\text{th}}^2$, and by zero elsewhere.

It is possible to increase the accuracy of the approximate integration by using a better approximation than a simple step. However, in order to keep the expressions manageable it seems reasonable to accept this choice as sufficient. It will be seen that the other factors in the integrand can be very well approximated in the regions where $B^2 > B_{\text{th}}^2$, which means that the main error in the approximate analytical result is the amplitude error close to the step. (Typically the amplitude is too high in the approximation.)

It should be noticed that it is not possible to set $k = l = m = 0$ in Eq. (4.22), i.e., this type of approximation cannot be used when studying SPM contributions. (There is no threshold value for B for SPM contributions, since there is temporal overlap from the start.) This is a minor problem since an alternative approximation is easy to obtain due to the fact that the exponential function in this case is much simpler; an approximation of the type (4.21) yields a solvable integral.

The factor involving the square root is approximated according to

$$\frac{1}{\sqrt{1+2iB+3B^2}} \approx \frac{1}{\sqrt{3B^2}} \frac{1}{1+\frac{i}{3B}} \approx \frac{1}{\sqrt{3B^2}}(1-\frac{i}{3B}) \approx \frac{1}{\sqrt{3B^2}} e^{-i\frac{1}{3B}}, \tag{4.23}$$

and the exponent in the last factor is approximated as

$$\exp\{\cdots\} \approx \exp\left\{ i\frac{\nu^2}{2B}\left[(k+l)^2-(k^2+l^2)\right]\right\} = \exp\left(i\frac{\nu^2 kl}{B}\right). \tag{4.24}$$

Inserting the resulting expressions into Eq. (4.17), the following approximate integral is obtained

$$\psi_p(L,t) = iA_0^3 \int_0^L \frac{\gamma p}{\sqrt{3}|B|} e^{i\frac{3\nu^2 kl-1}{3B}} H(B^2-B_{\text{th}}^2)\, dz, \tag{4.25}$$

where the exclusion of the negligible part has been indicated with Heaviside's step function $H(x)$.

4.3.2 General conclusions

A number of general conclusions can be drawn from Eq. (4.25). It is seen that if $B^2 < B_{\text{th}}^2$ everywhere, then there will be a negligible amount of nonlinear distortion. However, this cannot be realised with SMF and DCF since the fibre lengths will be limited to approximately $3L_D$.

The amplitude factor $1/|B|$ means that the amplitude asymptotically falls off in the same way for all contributions. The difference is that the step occurs for higher values of B^2 for contributions originating in signal pulses located further away from bit slot zero. It is therefore not obvious whether the strongest interaction takes place in i) regions of low B^2 with high amplitude and few contributions, or in ii) regions of high B^2 with low amplitude and many contributions. This important question is investigated carefully in Chapter 5, where it is found that the interaction can be of similar strength regardless of the value of B^2.

The integration in Eq. (4.25) is over z which runs over the entire system, but it is natural to make a variable substitution and integrate over B instead. It is then required that the integration is split into the regions of constant β_2, i.e., the different SMFs and DCFs. The integral in the arbitrarily chosen interval $[L_1, L_2]$ then becomes

$$iA_0^3 \int_{L_1}^{L_2} \gamma \cdots \, dz = i\frac{\gamma A_0^3 t_0^2}{\beta_2} \int_{B(L_1)}^{B(L_2)} \cdots \, dB. \tag{4.26}$$

If $\beta_2 < 0$ (which is the case for SMF) then $B(L_2) < B(L_1)$, and the negative sign of β_2 will be cancelled by the integral when the limits are exchanged. This shows that the SMF and DCF work together in adding to the total perturbation since there will be no cancellation of the nonlinear effects in different parts of the system. (If the system utilises precompensation, B can change its sign. Then the argument in Section 4.2.4 about cancellation of the imaginary part of the integrand applies.)

4.3.3 Approximate result

Using Eq. (4.25) it is possible to obtain an analytic approximation to the contribution corresponding to $(k, l, k + l)$. It is then assumed that the system has been split into regions with constant GVD parameter, which allows the total integral to be rewritten as a sum of integrals of the type in Eq. (4.26). For convenience it is assumed that $B(L_1) = 0$. Furthermore the attenuation must be set to zero for this final step. Since $\beta_2 < 0$ in an SMF, the final value $B(L_2) \equiv B_{\min} < 0$ and the integral

$$\int_0^{B_{\min}} \frac{1}{\sqrt{3}|B|} e^{i\frac{3\nu^2 kl-1}{3B}} H(B^2 - B_{\text{th}}^2)\, dB = \int_{B_{\text{th}}}^{B_{\min}} \frac{1}{\sqrt{3}B} e^{i\frac{3\nu^2 kl-1}{3B}}\, dB \tag{4.27}$$

can then be expressed in terms of the exponential integral[1] defined as

$$E_1(z) \equiv \int_z^\infty \frac{e^{-t}}{t}\, dt, \quad |\arg z| < \pi \tag{4.28}$$

and the resulting contribution is

$$\psi_p(L,t) = i\frac{\gamma A_0^3 t_0^2}{\sqrt{3}|\beta_2|}\left[E_1\left(i\frac{3\nu^2 kl - 1}{3|B_{\min}|}\right) - E_1\left(i\frac{3\nu^2 kl - 1}{\sqrt{3\nu^2(k^2+l^2-kl)-9}}\right)\right]. \tag{4.29}$$

The integration giving E_1 cannot be performed analytically. Instead the functions $iE_1(ix)$ and $iE_1(-ix)$ have been plotted in the complex plane using positive real arguments x in Figs. 4.2 and 4.3, respectively. Equation (4.29) constitutes one of the major results of this thesis, and is used extensively in Paper C to explain the obtained numerical results.

[1]The exponential integral (with this definition) is implemented in Matlab as `expint`.

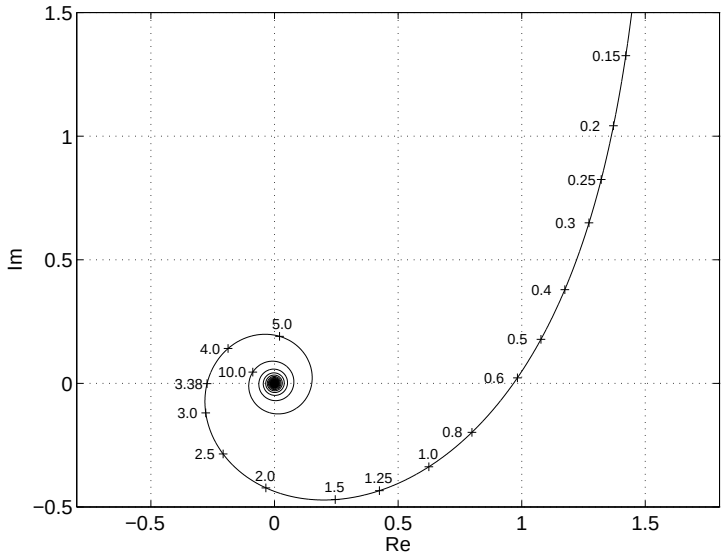

Figure 4.2: The function $iE_1(ix)$ in the complex plane using positive real arguments x. The value of the positive real argument x has been indicated at chosen points on the curve.

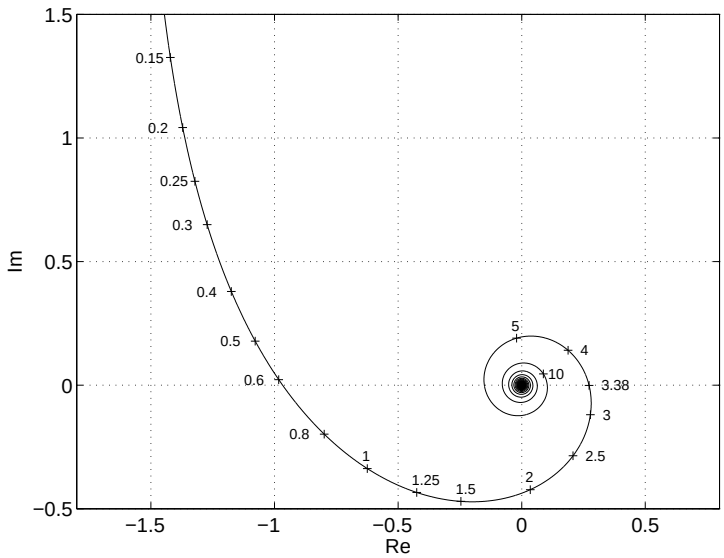

Figure 4.3: The function $iE_1(-ix)$ in the complex plane.

Chapter 5

Interaction range and strength

The accuracy of the perturbation analysis can be investigated by comparing the analytical results for individual contributions with numerical simulations. This has been done in Ref. [27], and it was found that the analysis is in good agreement with numerical results, although the XPM from the signal pulses leads to a systematic phase shift in the numerically obtained contributions. This shows the validity of the approximations made, but is not directly applicable to a real system where the total perturbation is built up from a large number of contributions. The interference process between different contributions is difficult to describe analytically, and the existing literature does not give a complete picture of this topic. Paper C, which is the result of an effort to describe this interference process, uses numerical simulations of the NLSE to obtain the nonlinear interaction, and the perturbation theory presented in Chapter 4 is then used to interpret the results. In particular, the interaction range of the nonlinear effects, i.e., the number of bit slots over which significant nonlinear interaction occurs, and the interaction strength, i.e., the generation rate of the nonlinear perturbation as a function of propagation distance, are discussed. These two concepts are introduced below.

5.1 Interaction range

It is known that the nonlinear interaction acts over many bit slots. In Ref. [20] it was found experimentally that the pseudorandom bit se-

quence (PRBS) had to contain on the order of 2^{20} pulses before the BER showed a convergent behaviour. The reported result is valid for a specific choice of system parameters and the generality is therefore limited, but the fact that the used system parameters are typical for a 40 Gbit/s channel shows that the interaction range can be very long in real systems. The result is important since most numerical system simulations are made using a much shorter PRBS [10,11,14,15,18,22,28–33], which can lead to an underestimation of the nonlinear effects. One of the main reasons for starting the work resulting in Paper C was to investigate the interaction range in detail and to provide analytical estimates that can be used for real systems.

Throughout Paper C the nonlinear interaction affecting a given bit slot, referred to as bit slot zero, is investigated. This bit slot carries either a zero or a one depending on whether ghost pulses or timing/amplitude jitter are being examined. In order to provide a convenient way of describing the surrounding bit train we use the words "symmetric" when the bit train has a mirror symmetry in bit slot zero, and "asymmetric" when the bit train contains no signal pulses in bit slots with negative indices. When investigating the interaction range the nonlinear perturbation is plotted as a function of N, which denotes the length of the bit train; when the length is N it means that bit slots with indices $1 \leq n \leq N$ contain signal pulses. In all simulations sufficiently many empty bit slots are added to avoid effects from the implied periodicity of the numerical simulation.

An example result for a lossless system taken from Paper C is seen in Fig. 5.1, which shows the amplitude of the ghost pulse in the middle of the studied bit slot using symmetric bit trains, i.e., the bit slot is empty and is surrounded by N signal pulses on each side. The different curves correspond to a fibre length of $L = 50$, 100, 150, and 200 km. It is known that a high N typically generates a strong ghost pulse [10,20], but it is seen in Fig. 5.1 that, e.g., $N = 24$ leads to an even stronger ghost pulse in the case of a 200 km fibre. The interaction range is the value of N where the result is starting to show a convergent behaviour. This definition is unfortunately not strict, but the value of N at the peak is a reasonable indication of the needed word length. It is seen that with a 100 km fibre, $N > 12$ is needed to pass the peak. However, deviations of less than 10% of the final value are not seen until $N > 25$. As is discussed in Paper C, a sufficiently long PRBS, i.e., a PRBS which will give rise to a converged BER, must in this case contain 2^{51} pulses.

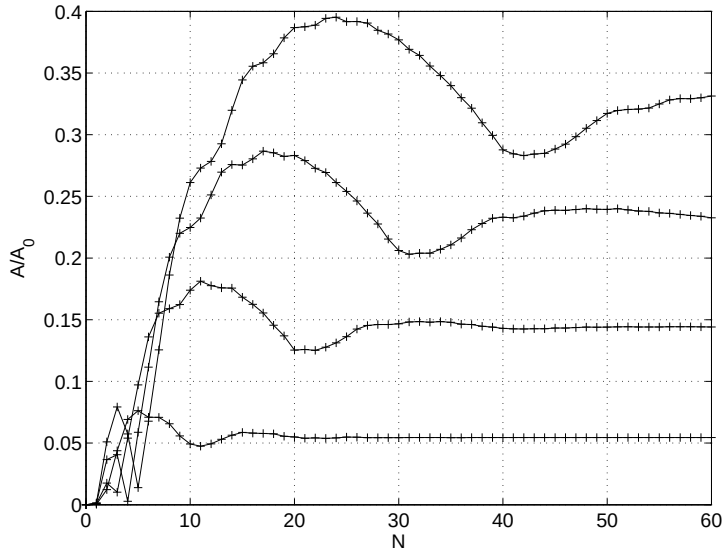

Figure 5.1: The ghost pulse amplitude using different symmetric pulse trains with an SMF of length (from below) $L = 50$, 100, 150, and 200 km.

However, the effect from attenuation is important since it can limit the interaction range considerably, and this is further discussed below.

The perturbation analysis from Chapter 4 is used in Paper C to explain the location of the global maxima of Fig. 5.1 using the fact that the contributions to the total perturbation eventually start to interfere destructively as N increases. In this way it is possible to predict the locations of the peaks, and an estimate for the value of N where the peaks are located is given by

$$\frac{3\nu^2 kl - 1}{3|B_{\min}|} \approx \frac{\nu^2(N-1)}{|B_{\min}|} \approx 3.38. \tag{5.1}$$

(It should be remembered that $B_{\min} < 0$ since an SMF is considered.) The results are $N = 7$, 12, 18, and 23, respectively, for the different fibre lengths in Fig. 5.1. Equation (5.1) constitutes a simple analytical way of predicting the interaction distance, although it should be noticed that a small error in the interaction range estimate leads to a large error in the predicted PRBS length due to their exponential relation.

It is interesting to see that the analysis can be used to explain almost all details of the interaction. As an example the curve for the 200 km

long fibre in Fig. 5.1 is seen to be close to zero for $N = 5$, and the reason is explained in Paper C using simple interference arguments. The fact that the closest neighbours to bit slot zero (typically $N < 3$) lead to contributions that interfere destructively when N is increased from 3 to 5, suggest that a larger ghost pulse could be obtained by leaving the closest bit slots empty. This argument is however incorrect, since the pulses in these bit slots participate in many contributions that are important in building up the ghost pulse.

The amplitude and timing jitter are investigated in a similar manner in Paper C. It is found that a short array of ones generates the strongest amplitude jitter and the worst case for timing jitter is a semi-infinite array of ones starting in bit slot zero. With the current choice of system parameters the amplitude and timing jitter counteract each other, which leads to partial cancellation of the nonlinear effects. By changing the sign of β_2 (in all fibres of the system) the opposite effect is seen; the amplitude and timing jitter work together in decreasing the pulse amplitude. This shows that the amount of nonlinear intrachannel effects depends on the sign of the dispersion.

From the numerical simulations it can be concluded that XPM does not cause any significant amplitude jitter. This has been confirmed by two observations. Firstly, the case $N = 1$, corresponding to one single contribution caused by XPM, has been found to generate little amplitude jitter. Secondly, by phase shifting every second bit slot (using the alternate-phase return-to-zero modulation format, see Chapter 6) it is seen that the amplitude jitter oscillates as N increases. Since the XPM contributions are not affected by phase shifting it is clear that the generating effect is not XPM.

5.1.1 The effect of attenuation

When the attenuation is neglected, the minimum value of the accumulated dispersion should be used in Eq. (5.1). The predicted interaction range is then typically very long, and it is emphasised that with a given dispersion map the predicted value of the interaction range is always possible to reach by placing an amplifier close to the region in which B^2 attains its maximum value. However, if the system is designed to carry high power only in regions of small pulse overlap, the interaction range will be suppressed.

As is seen from Eq. (4.16) the local value of the pulse power acts as a weighting function for the nonlinear interaction. When approximating

Eq. (4.17) in order to obtain Eq. (4.29) the non-overlapped parts were excluded by the use of Heaviside's step function. A similar, somewhat crude, approximation is suitable here and provides a convenient way of thinking of the effects of attenuation. Thus, p (see Eqs. (2.14) and (4.16)) is approximated by either one or zero, depending on whether the pulse power is above a certain threshold, and the value for $B_{\min}$ should be optimised within the regions of the system where the power level is above the threshold.

Paper C contains an analytical estimate of the interaction range of the system considered in Ref. [20]. Since the system is precompensated, the maximum power occurs at a large value of B^2 and this value should be used for the range prediction. However, as also discussed, a more difficult situation arises if the regions of high power coincide with low values of the accumulated dispersion. As mentioned above it is in this case necessary to define a threshold value, which is a somewhat arbitrary process. As proposed in Paper C, using $p = 0.1$, corresponding to 10% of the maximum power, is reasonable.

5.2 Perturbation growth

The asymptotic behaviour of the function $E_1(ix)$ is logarithmic when $x \to 0$, and by studying a chosen, single contribution it is found that the growth rate is small when B^2 is large. This has lead to the suggestion that the nonlinear perturbation can be made small by designing the dispersion map in such a way that the pulses are strongly overlapping everywhere except close to the transmitter and receiver [22]. This is however true only as long as very short pulse trains are considered. In a long pulse train many contributions are generated, and the fact that they tend to align their phases (see Paper C) implies that the interference is constructive.

One of the main goals of Paper C is to compare the growth rate of the nonlinear perturbation at different values of B in order to see if high accumulated dispersion leads to weak interaction. This has been done by simulating the NLSE numerically in the following way: The initial field is propagated a given distance. The accumulated dispersion in the obtained field is compensated for using a linear, lossless DCF and sampled, giving the local value of the perturbation. The (non-compensated) field is then further propagated according to the NLSE, and the process is iterated until the end of the SMF is reached. This gives the pertur-

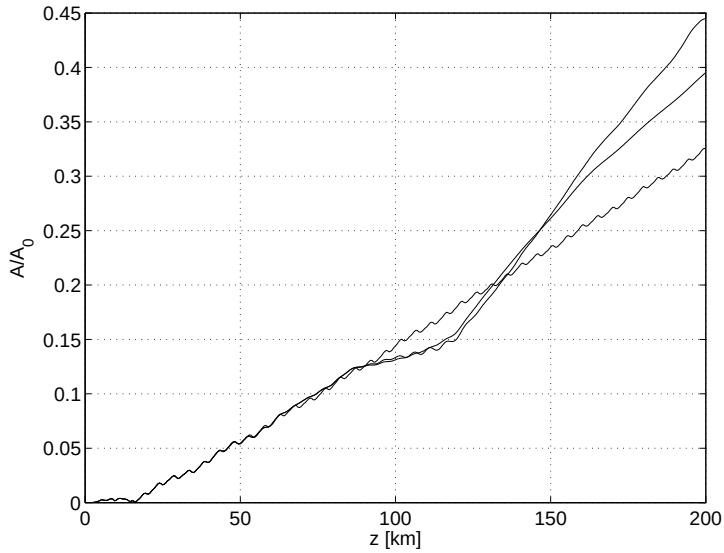

Figure 5.2: The ghost pulse amplitude as a function of propagation distance. The different curves are described in the text.

bation as a function of propagation distance, or, stated differently, the perturbation that would be generated if the system was terminated and dispersion compensated at the given propagation distance.

Figure 5.2 shows a numerical simulation of the growth of the amplitude of a ghost pulse along a single, lossless SMF using symmetric bit trains. The numerical parameters used are stated in Paper C. The curve ending with a value of roughly 0.32 corresponds to a bit train consisting of a single zero between ones. It is seen that the growth rate is similar at all except the lowest values of L (corresponding to small B^2). The initial region of weak interaction corresponds to the region of small pulse overlap. The oscillations along the curve are created when contributions corresponding to larger values of $|kl|$ interfere with the total perturbation during the last turn in the spiral-shaped part of E_1.

The threshold value for L where the linear growth starts corresponds to the fibre length where the closest neighbours to bit slot zero are partially overlapping. In terms of Figs. 4.2 and 4.3 this means that the strongest contribution has left the spiral-shaped part of E_1 and is approaching the logarithmic region. Using the fact that the strongest contribution has $|kl| = 1$ (occurring for, e.g., $(1, 1, 2)$), the threshold

occurs when the argument in Eq. (4.29) is

$$-i\frac{3\nu^2 kl-1}{3B}\approx -i\frac{\nu^2}{B}\approx -2i, \tag{5.2}$$

giving

$$L\approx \frac{T_B^2}{2\beta_2}\approx 15 \text{ km}. \tag{5.3}$$

It has been reported several times in the literature that the strongest ghost pulses tend to appear between long sequences of ones [10,20]. However, the interference process leading to the ghost pulse is complicated and, as seen in Fig. 5.1, the amplitude of the ghost pulse oscillates as N increases. It is clear that the case $N\to\infty$ is not the worst case, and by using a symmetric pulse train with $N=24$, i.e., the pulse train is

$$\ldots 000\underbrace{111\ldots111}_{24}0\underbrace{111\ldots111}_{24}000\ldots,$$

the curve ending at 0.39 in Fig. 5.2 is obtained. This corresponds to truncating the pulse train before the interference becomes destructive.

The fact that the contributions in the spiral-shaped region of E_1 can interfere both constructively and destructively with the total perturbation implies that by starting from the $N=24$ case and including a sequence of ones located further away from bit slot zero, constructive interference can again be obtained. This results in the curve in Fig. 5.2 ending at 0.44, i.e., the amplitude is more than 30% larger than in the case of an infinite train of ones. It should thus be concluded that the case of a single zero between a long sequence of ones is a reasonable indication for the worst case, but the difference can be significant.

The effect of changing some system parameters has been investigated in Paper C. If the pulse width is changed and the pulse energy is held constant (by adjusting the peak power level) the perturbation analysis predicts $|\psi_p|\propto\sqrt{t_0}$, and this has been confirmed using numerical simulations. It is well known that a smaller pulse width leads to weaker nonlinear interaction [5, 23], but in practise there are small possibilities for such adjustments since a more narrow pulse is more difficult to generate and also has a larger bandwidth, leading to lower spectral efficiency at a given bit rate.

The effect of changing the dispersion parameter is illustrated in Fig. 5.3 where the ghost pulse for a bit train with a single zero between ones has been plotted for a dispersion parameter that is 1/4, 1/2,

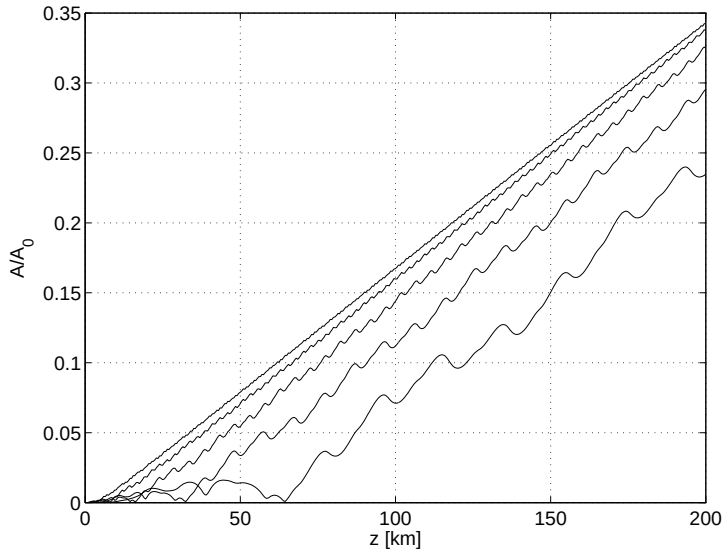

Figure 5.3: The ghost pulse amplitude as a function of propagation distance using (from below) a GVD parameter $\beta_2/4$, $\beta_2/2$, β_2, $2\beta_2$, and $4\beta_2$.

1, 2, and 4 times the value in Fig. 5.2. It is seen that the growth rate is similar in all cases but in the case of a small dispersion parameter the start of the significant interaction, which occurs when there is partial overlap between the signal pulses, is delayed to a later position in the fibre. This is a somewhat unexpected result since the fact that a smaller pulse width (and a faster pulse broadening) leads to weaker interaction suggests that a higher dispersion could have a similar impact. In Ref. [23] it is stated that the fast spreading of the pulses in the time-domain can combat the nonlinear effects. However, the results presented here show that for ghost pulses this argument can only be applied to the width of the pulses and cannot be used when discussing the value of the dispersion. In the case of timing jitter, a large GVD parameter can be beneficial, since the timing jitter tends to be averaged out when many pulses participate in the interaction, but the impact in the worst case (an asymmetric pulse train) would not be decreased.

The fact that the growth rate of the perturbation can be similar at most values of B has implications for the possibilities of counteracting the nonlinear interaction; except for the initial region of no signal pulse

overlap, it should be of little consequence whether the pulses are strongly or weakly dispersed during propagation (without leaving the pseudolinear regime) or if the amplifier locations are changed. These results imply that it is in general hard to suppress the ghost pulses by designing the dispersion map and choosing the (lumped) amplifier positions. More promising methods include using different modulation formats, e.g., the alternate-phase return-to-zero modulation format (see Chapter 6) format which uses phase shifting to induce destructive interference between different contributions.

We emphasise that the result obtained here applies to the worst case. Ref. [15] reports that, e.g., the timing jitter, defined as the standard deviation of the temporal location of the signal pulses, decreases when the value of the GVD parameter is increased. This is a reasonable result since most pulses will be affected by the attraction from many pulses, and the result is that the timing jitter tends to be averaged out. On the other hand, Ref. [32] finds that also the worst case, defined as the maximum eye-opening penalty, has a maximum value for a certain value of the GVD parameter. This value happens to correspond to a system using SMF and a channel speed of approximately 40 Gbit/s. However, the word length used both in the numerical simulations and in the experiments is only 128 bits, and this makes the results questionable, since, e.g., the sequences generating the strongest timing jitter will not be present in such a bit train.

The last part of Paper C discusses the effect from precompensation, and the results are in accordance with earlier published material. Thus, it is seen that the ghost pulses cannot be efficiently suppressed, but the amplitude and timing jitter can be reduced considerably by using a properly designed dispersion map. In the case of ghost pulses, see Fig. 5.4, the small effect seen is due to the fact that the propagation distance in the region of no pulse overlap is twice as long when precompensation is applied. Using the perturbation analysis it is predicted that the two cases of full and no precompensation, which also corresponds to changing the sign of β_2 (in all fibres of the system), should yield identical perturbations. The difference seen between the corresponding two curves in Fig. 5.4 is due to the fact that the perturbation ansatz is beginning to fail since the perturbation is not much smaller than the signal pulse anymore. By decreasing the pulse power and recalculating the data shown in the figure it is seen that the final values approach each other.

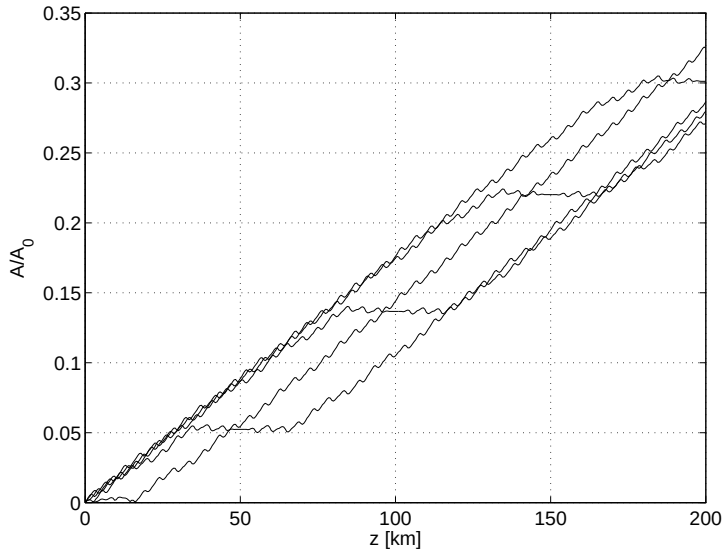

Figure 5.4: The ghost pulse amplitude as a function of propagation distance using different amounts of precompensation. Counting the horizontal parts of the curves from below the length of the precompensating DCF is 0, 1/4, 1/2, 3/4, and 1 times the length of the SMF.

It is found that in the unattenuated case the optimum precompensation is different for the two effects of amplitude and timing jitter. When attenuation is included it is still possible to counteract these effects efficiently, but the optimum amount of precompensation must then be found from numerical simulations of the given system.

Chapter 6

Suppression methods

Nonlinear signal distortion decreases the OSNR and must be controlled in order to increase the bit rate. The system development process can then either i) be focussed on finding suppression methods which allow higher power levels or ii) accept the power restrictions and instead try to increase the sensitivity of the system. One example of the former is to use precompensation in order to counteract the generation of nonlinear effects, which has already been discussed. Here, a suppression scheme is presented that is based on phase shifting of the signal pulses. The technique is called *alternate-phase return-to-zero* (APRZ) and the results have been reported in Papers D and E. This method of suppression was also independently suggested in Ref. [34].

Since the introduction of phase shifts can be viewed as switching to a modified data modulation format (DMF), an overview of alternatives to the OOK DMF will first be given with special emphasis on the tolerance to nonlinear effects. Then the reason for the robustness to nonlinear distortion of the APRZ DMF is discussed thoroughly, and finally a number of other suppression methods proposed in the literature are described together with relevant references.

6.1 Alternative modulation formats

The OOK DMF, i.e., binary intensity modulation with a bit encoded either as the presence or absence of a signal pulse, has traditionally been the DMF of choice due to the technical complications of more advanced modulation formats. This situation is however changing and today there are several alternative DMFs which lead to improved system

performance [1]. The brief overview presented here describes a number of DMFs that introduce additional modulation of the light without changing the method of encoding the carried data. This is done in order to increase the tolerance to signal distortion. Only DMFs where the data is encoded in the intensity are presented since these are more directly comparable with the OOK DMF. No NRZ modulation formats will be considered.

Carrier-suppressed return-to-zero (CSRZ) is OOK with additional phase shifting; there is a π phase jump between all neighbouring bit slots. Due to the generation method, the duty cycle of CSRZ is typically 67% if additional intensity modulation is not carried out [1]. CSRZ has numerically and experimentally been found to increase the tolerance to nonlinear effects [35–39].

In the chirped return-to-zero (CRZ) DMF there is a phase modulation within the bit slot that imposes a chirp on the signal pulses [1]. This will broaden the spectrum and decrease the spectral efficiency, but this effect can be counteracted by using the alternate-chirp return-to-zero (ACRZ), in which the phase is modulated to make the sign of the chirp change between neighbouring bit slots [40]. In an experimentally implemented case, APRZ will also create a small (alternating) chirp on the signal pulses, and APRZ becomes similar to ACRZ when the phase shift is chosen to be π. Some authors actually refer to ACRZ as "APRZ". A small increase in robustness to fibre nonlinearity has been seen experimentally in WDM systems in the case of CRZ [41], and the nonlinear tolerance of ACRZ has been reported to be superior to CSRZ [40]. CRZ can also be modified by using CSRZ pulses [42].

The duobinary (DB) and the alternate-mark inversion (AMI) DMFs both introduce correlation between the data and the phase of the field; in DB the phase of the signal pulse is changed if there are an odd number of zeroes between the current and the last ones, and in AMI the phase is changed at all ones [1]. These DMFs are both capable of increasing the dispersion tolerance, which can be realised by studying the bit sequence one, zero, one; the signal phase shifts of the pulse will cause destructive interference in the middle bit slot. An increased tolerance to nonlinear effects has also been reported [39, 43–46][1].

The APRZ DMF can be considered to be a generalisation of the CSRZ, since the phase jump can be chosen arbitrarily. However, some authors consider APRZ to be a generalisation of ACRZ due to the fact

[1]Note that ACRZ is referred to as APRZ in Refs. [43] and [46].

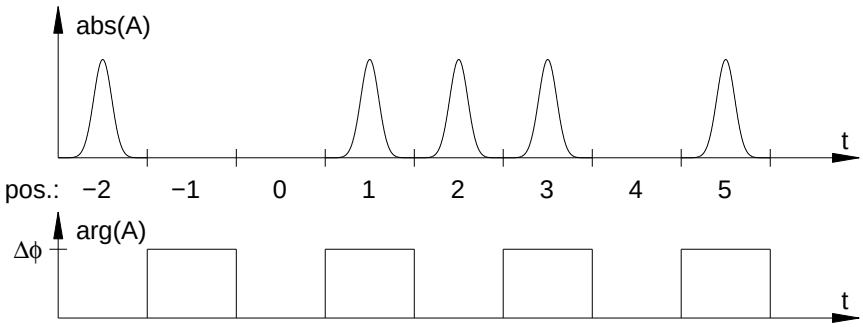

Figure 6.1: Initial amplitude and phase modulation of a bit stream.

that in an experimentally implemented APRZ data signal a certain amount of chirp is imposed on the pulses. Experimental results have shown that APRZ is capable of efficient suppression of the nonlinear distortion [33, 39, 47, 48], and APRZ seems to outperform all the above given alternatives to OOK. A possible extension of APRZ is to combine the phase shifting with polarisation shifting [49]. A thorough description of the reason for the tolerance to nonlinear effects of APRZ DMF will be given below.

It should be noticed that, e.g., in the case of CSRZ it is hard to find an analytical explanation for the found increase in tolerance to nonlinear effects. The following analytic treatment of the APRZ DMF contains CSRZ as a special case (when the phase shift is chosen to be π), but in this case the resulting nonlinear distortion is predicted to be the same as without phase shift. Although unsatisfactory, this is not the only issue of similar status; a similar case is why the nonlinear tolerance of RZ is superior to NRZ at high channel data rates [5, 7, 8]. However, it can be considered to be an advantage of the APRZ DMF that there is a reason why, e.g., the case of $\pi/2$ phase modulation should be expected to show different nonlinear tolerance than OOK.

6.2 The alternate-phase return-to-zero DMF

The generation of ghost pulses and amplitude jitter is a phase sensitive process. This implies that the nonlinear interaction is affected by a phase shift of the type seen in Fig. 6.1, and it has been found that a suppression of the nonlinear distortion is possible to obtain. Although

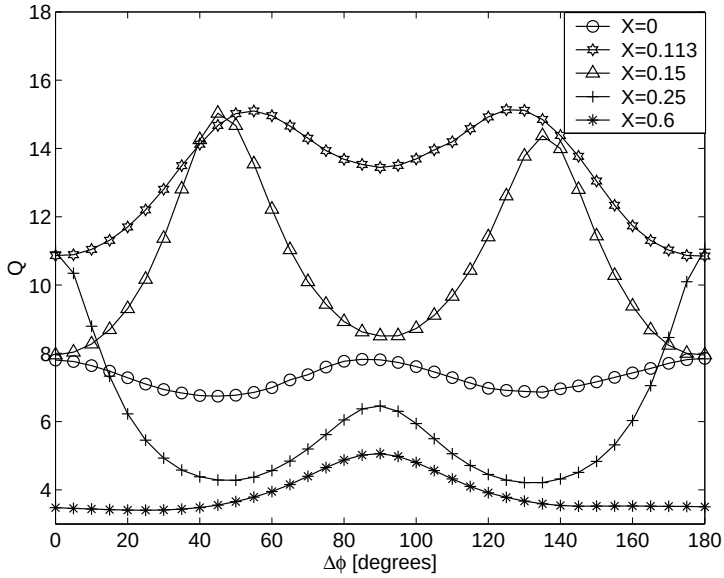

Figure 6.2: The Q-value as a function of phase shift, $\Delta\phi$, and launch position, X. It is seen that phase shifting can improve or decrease the signal quality. Notice the symmetry around $\Delta\phi = \pi/2$.

the choice of possible phase-shifting schemes is limited to physically realizable signals, it is convenient to use the idealised scheme in Fig. 6.1 to explain the suppressive effect theoretically. This type of phase shifting scheme, which is called APRZ, shifts the phase of every second signal pulse by $\Delta\phi$.

In simulations of systems using the APRZ DMF it is seen that the Q-value is changed when $\Delta\phi$ is adjusted, and generally the system performance is increased when $\Delta\phi$ is optimised properly. Figure 6.2 shows a number of simulations for a system with 20 DM cells. Each DM cell consists of one SMF ($L = 50$ km, $D = 16$ ps/(nm×km)) and one DCF ($L = 10$ km, $D = -80$ ps/(nm×km)) and there is one noise-free fibre amplifier in each DM cell to compensate for fibre losses. The different curves correspond to different launch positions. It is seen that the Q-value can be greatly increased by combining a proper phase shift and launch position. In Fig. 6.2 it is also seen that there is a symmetry around $\Delta\phi = \pi/2$, i.e., $Q(\pi/2-\Delta\phi) = Q(\pi/2+\Delta\phi)$, and that $Q(\Delta\phi)$ is periodic with period π, and the reason for this will be explained below using the perturbation analysis.

k	l	$m = k + l$	φ
even	even	even	0
even	odd	odd	0
odd	even	odd	0
odd	odd	even	$2\Delta\phi$

Table 6.1: The phase shift, φ, of the (k, l, m) contribution depends on whether k, l, and m are odd or even. It is assumed that all odd bit slots are phase shifted.

6.2.1 The symmetries

By using APRZ the signal pulses in odd bit slots will be multiplied by $e^{i\Delta\phi}$. The shift of the (k, l, m) contribution will, due to linearity, be the same as the shift of the corresponding source term. This, in turn, depends on whether k, l, and m are odd or even. When bit slot zero is studied we demand that $k + l - m = 0$. All possible situations in this case are found in Table 6.1, and it is seen that if k and l are both odd the phase of the contribution will be shifted $2\Delta\phi$. No other contributions are affected. This is the reason why the period in the Q-value plot is π instead of 2π.

There are now two groups of contributions to the total perturbation. The first group consists of those that are not affected by a phase shift, and the second contains those that are shifted $2\Delta\phi$. By summing the contributions in the two groups separately, two phasors are obtained, which have been plotted qualitatively in Fig. 6.3a. The effect from a phase shift $\Delta\phi$ is seen in Fig. 6.3b; one of the phasors is stationary in the complex plane and the other rotates an angle $2\Delta\phi$. It is clear that by choosing $\Delta\phi$ suitably, the contributions can be made to counteract each other. Thus the suppressive effect is due to destructive interference between the different contributions to the nonlinear effects.

To understand why there is a symmetry of the Q-value around $\Delta\phi = \pi/2$ a phase-shifted bit slot has to be examined. If bit slot number zero is still studied it should then be assumed that all even bit slots are phase shifted, and the results listed in Table 6.2 are obtained. Since the phase of the signal is $\Delta\phi$ the result is identical when k or l is even. However if k and l are odd the shift of the contribution is $-2\Delta\phi$ relative to the signal, which means that the shifted contributions rotate in the other direction in a phase shifted bit slot. This is seen in Fig. 6.3c. When

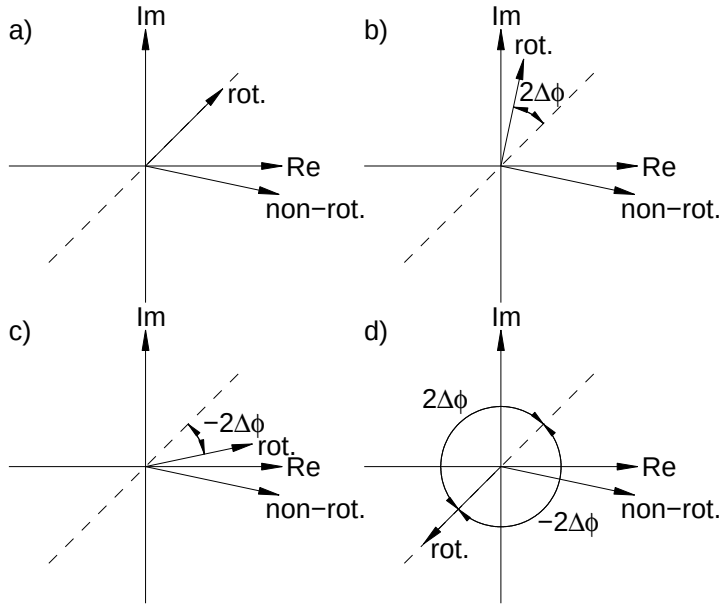

Figure 6.3: a) The rotating and non-rotating phasors when $\Delta\phi = 0$. b) A phase shift $\Delta\phi$ gives a rotation 0 or $2\Delta\phi$. c) The situation in a phase shifted bit slot. The direction of rotation is changed. d) $\Delta\phi = \pi/2$. All bit slots are identical.

$\Delta\phi$ is a multiple of $\pi/2$ this implies that all bit slots are affected in an identical way as illustrated in Fig. 6.3d. It should be expected that the Q-value is symmetric around $\Delta\phi = 0$, since a positive or negative phase shift should give the same effect. (Only the relative phase between the signal pulses is important and a shift $\Delta\phi$ of the odd bit slots is equivalent to a shift $-\Delta\phi$ of the even bit slots.) It is realised from Figs. 6.3a and d that the same kind of symmetry argument should apply also around the value $\Delta\phi = \pi/2$.

6.2.2 Simulations of individual contributions

In order to clearly show the effect of the phase shift, numerical simulations have been carried out. A number of calculated (complex) contributions to a ghost pulse have been plotted in Figs. 6.4 and 6.5 using $\Delta\phi = 0$ and $\Delta\phi = \pi/2$. The different contributions are marked with the generating source term. In order to isolate one particular contribution

k	l	$m = k + l$	φ
even	even	even	$\Delta\phi$
even	odd	odd	$\Delta\phi$
odd	even	odd	$\Delta\phi$
odd	odd	even	$-\Delta\phi$

Table 6.2: The phase shift, φ, of the (k, l, m) contribution in bit slot zero if all even bit slots are phase shifted.

in the numerical simulation only those signal pulses that give rise to the contribution of interest are included in the pulse train, and this is repeated for all the needed contributions. The system parameters from Section 3.4 has been used and the full NLSE has been simulated.

Among the included contributions there are three for which both k and l are odd: $(1, 1, 2)$, $(-1, 3, 2)$, and $(1, 3, 4)$. The analysis predicts them to be rotated $2\Delta\phi$ when APRZ is applied, and by comparing Figs. 6.4 and 6.5 it is seen that with $\Delta\phi = \pi/2$ they are rotated π. No other contributions are phase shifted and the amplitudes are more or less unaffected by the phase shift. The small deviations from the theoretical predictions seen, e.g., in $(-1, 2, 1)$ are due to the limited accuracy of the perturbation approach.

6.2.3 Interaction range simulations

In Section 5.1 the interaction range was computed analytically and numerically and illustrated by plotting the ghost pulse amplitude, the signal pulse amplitude, and the timing jitter as a function of the bit train length N. Similar plots corresponding to Figs. 2–5 in Paper C using APRZ with $\Delta\phi = \pi/2$ are found in Figs. 6.6–6.9. (The plot of the timing jitter has not been included since the XPM interaction is not affected by a phase shift.) In all cases it is seen that the curves oscillate as N increases, which is a sign of the destructive interference between contributions with similar values of k and l. This result is expected from the above phase shift arguments and provides further support for the claim that APRZ can suppress the nonlinear distortion.

As seen in Fig. 6.6 the maximum ghost pulse amplitude is less than half compared to the case reported in Paper C with no phase shifting. This is an indication that the APRZ DMF is capable of a substantial reduction of the nonlinear distortion. Good suppression is also seen in

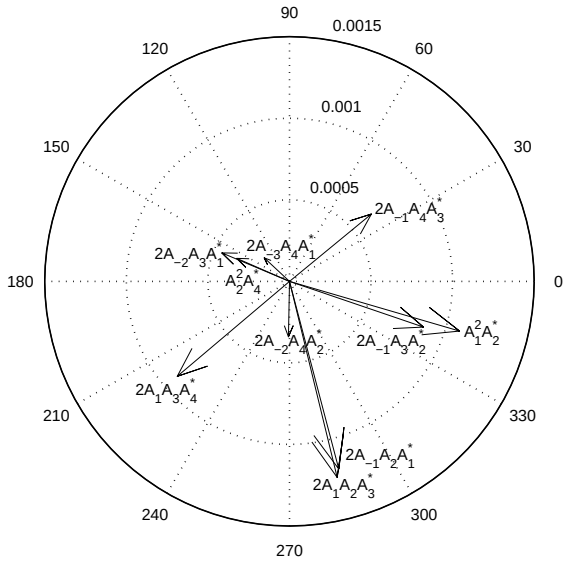

Figure 6.4: Complex contributions to a ghost pulse when $\Delta\phi = 0$. The phasors are contributions and they are marked with the generating source term.

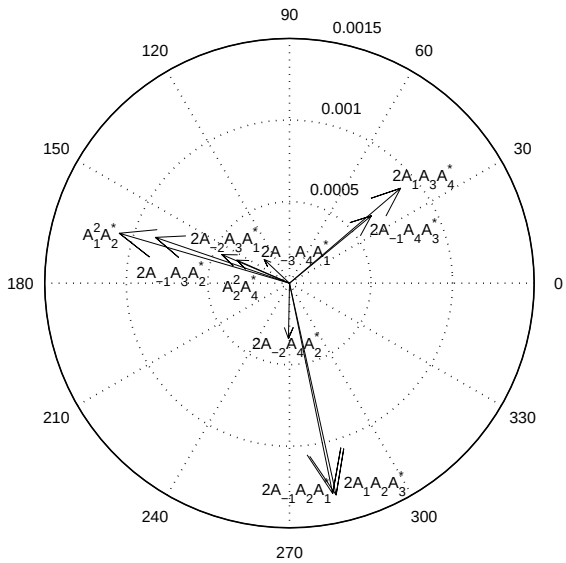

Figure 6.5: Contributions to a ghost pulse when $\Delta\phi = \pi/2$.

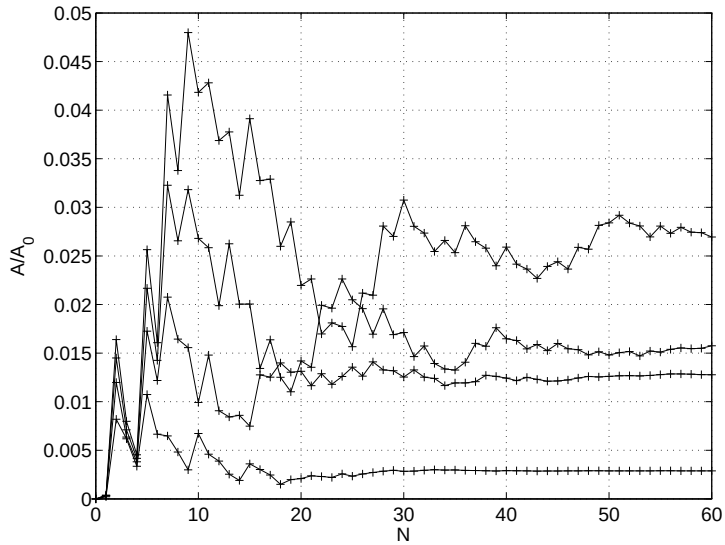

Figure 6.6: The ghost pulse amplitude using asymmetric pulse trains with SMF of length (from below) $L = 50$, 100, 150, and 200 km. APRZ with $\Delta\phi = \pi/2$ is used.

the amplitude jitter using an asymmetric bit pattern, but in the case of a symmetric bit pattern the worst case occurs for $N = 2$. Thus, the amplitude jitter is caused by few contributions but the destructive interference between contributions can only counteract the buildup of a strong total perturbation efficiently. However, with phase shifting the amplitude jitter is of more similar strength in the cases of symmetric and asymmetric pulse trains.

6.3 General phase shifting

In APRZ all pulses have phase shifted closest neighbours, next closest neighbours with the same phase etc. This is true regardless of whether the studied bit slot is phase shifted or not. Thus there is a certain type of translational symmetry in APRZ. It is interesting to study whether there are other phase shifting schemes that keep this certain symmetry, i.e., the phase shifting affects all bit slots in the same way. It is possible to find all shifting schemes with this symmetry, and the result is that there are only two; the first is APRZ and the second is *pairwise*

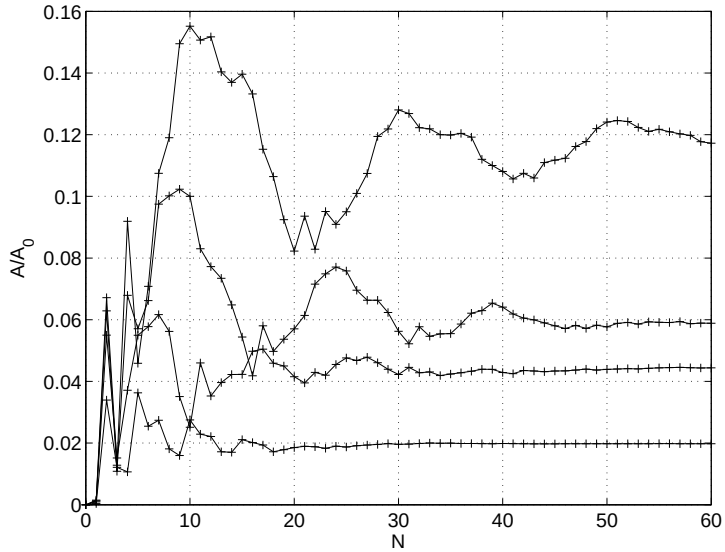

Figure 6.7: The ghost pulse amplitude using symmetric pulse trains with SMF of length (from below) $L = 50$, 100, 150, and 200 km. APRZ with $\Delta\phi = \pi/2$ is used.

alternate-phase return-to-zero (PAPRZ) in which the bit slots are shifted $(\ldots, 0, 0, \Delta\phi, \Delta\phi, 0, 0, \Delta\phi, \Delta\phi, \ldots)$ instead of $(\ldots, 0, \Delta\phi, 0, \Delta\phi, \ldots)$. It has been found that PAPRZ has similar suppressive effect [50], but should be easier to implement due to the lower frequency. In Ref. [34] a numerical study that compares different phase shifting schemes is reported. In short, a two-dimensional space of different schemes is examined and the best suppression is obtained in the two cases APRZ and PAPRZ, respectively. This provides partial support for the claim that these two types of phase shifting are special.

With APRZ it was found that each (k, l, m) contribution was phase shifted in one of two possible ways. With PAPRZ the contribution can be shifted in any of the four possible ways, $-\Delta\phi$, 0, $\Delta\phi$, or $2\Delta\phi$. This means that with PAPRZ the period will be 2π in a plot of, e.g., the Q-value as a function of $\Delta\phi$. The symmetry around $\Delta\phi = \pi/2$ will not appear in PAPRZ, since it in the APRZ case is due to the fact that all bit slots are affected identically by a phase shift $\Delta\phi = \pi/2$.

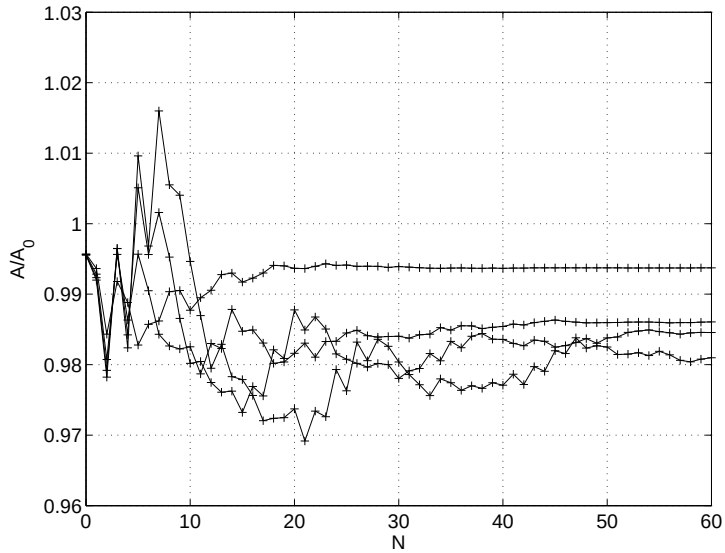

Figure 6.8: The total pulse amplitude using asymmetric pulse trains with SMF of length (from above) $L = 50$, 100, 150, and 200 km. APRZ with $\Delta\phi = \pi/2$ is used.

6.4 Other suppression techniques

The suppressive effects that can be obtained from precompensation and phase shifting have been presented, but similar effects can also be obtained by tailoring other system parameters such as the frequency, the pulse spacing etc. This has been the starting point for a number of alternative suppression techniques, which are briefly presented below.

6.4.1 Bit stream depending modulation

As already shown, the choice of a proper DMF is important in order to counteract the generation of nonlinear signal distortion effectively. However, it is likely that the nonlinear distortion will continue to be a significant limiting factor and ultimately there might be a need for more drastic measures to reduce them. One such measure is to introduce data dependent phase shifting. By numerical simulations of a given system it is possible to find how specific patterns in the data stream should be phase encoded in order to maximise the suppression on nonlinear effects.

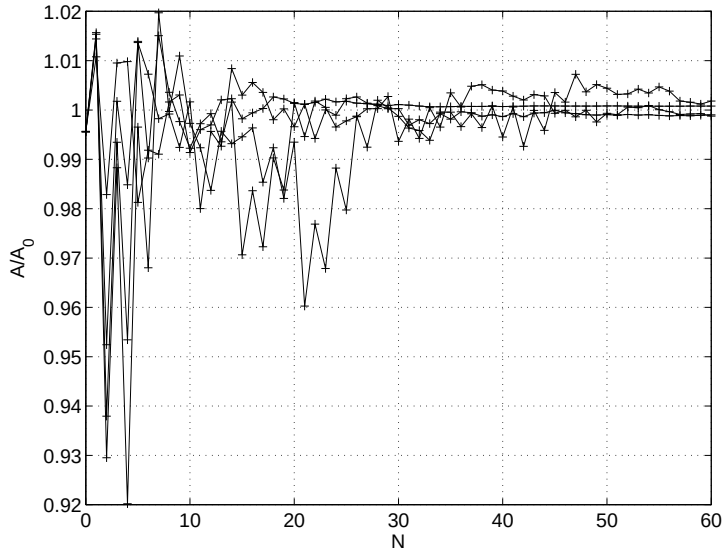

Figure 6.9: The total pulse amplitude using symmetric pulse trains with SMF of length (from below at the maxima) $L = 50$, 100, 150, and 200 km. APRZ with $\Delta\phi = \pi/2$ is used.

As is shown in Ref. [51] this can potentially reduce the nonlinear impairment drastically, but the experimental complications of such a scheme are obvious. A different suggestion is to avoid sequences known to cause strong nonlinear effects by using line coding [52]. Sequences known to cause problems are then simply forbidden and the data is encoded using permitted sequences. Apart from the need for signal processing to encode the data into permitted sequences this method also decreases the data rate (at a given channel bit rate) slightly, depending on the number and length of the forbidden sequences. Both these methods are reported to improve the Q-value with more than 4 dB.

6.4.2 Subchannel-multiplexed systems

A scheme where the frequency instead of the phase of the signal pulses is changed between neighbouring bit slots has been found to have a suppressive effect on the nonlinear effects [53]. These systems are called subchannel-multiplexed since two signals from two lasers operating at different wavelengths will be multiplexed in time.

This scheme will increase the bandwidth of the signal, giving rise to

a trade-off between spectral efficiency and nonlinear impairment. Significant reduction of the amplitude jitter has been seen, but frequency separations as large as 200 GHz are considered, and this is much more than the bandwidth of the signal. It is also found that at certain frequency differences there are resonances in the amplitude jitter generation, which gives rise to stronger nonlinear effects. Another drawback is the practical complications from the need for two lasers per channel, as well as complex electro-optic modulation and detection.

6.4.3 Unequal pulse spacing

In Ref. [26] it has been suggested that temporal shifting of the signal pulses can decrease the effect of the Kerr nonlinearity. This can be implemented using time division multiplexing and adjusting the delay for the different channels, but it will sacrifice some spectral efficiency and complicates the decoding of the signal. A perturbation analysis was used to study amplitude jitter in the form of power transfer between three pulses. Using 40 Gbit/s one pulse is located at $t = 0$ and one at $t = 25$ ps. The temporal position of the third is varied between $t = -25$ ps and $t = -12.5$ ps. With the largest shift the power transfer is reduced to a quarter of the value with no shift after propagation through an 800 km system. Using a shift of 7.5 ps a 3 dB improvement of the Q-value is found in the same system.

Chapter 7

All-optical regeneration

The signal distortion increases during the transmission due to the accumulation of amplifier noise and other effects that are not compensated for, e.g., nonlinear effects, TOD, and PMD. This eventually leads to bit errors, but the accumulation process can be counteracted by using signal regeneration. Here, a short overview of the basic concepts of regeneration is given, and all-optical regeneration of OOK and differential phase-shift keying (DPSK) data is discussed together with an introduction to Papers F and G.

7.1 Signal regeneration

A regenerator can be considered to consist of a receiver followed by a transmitter. The receiving part must be properly designed in order to avoid misinterpretation of the incoming data pulses, and the obtained data stream is then fed to the transmitter which encodes the information into light in a signal that can have arbitrarily high quality. This way of viewing the regenerator closely follows the traditional way of implementing a regenerator, in which an electronic receiver is followed by a laser and modulation equipment that generates the new pulse train. The drawback of this (otherwise well-working) scheme is the speed limitation of electronic devices, and as the bit rates are increased in order to make better use of the bandwidth of the optical fibre, a need for faster regeneration arises. The problem can be solved by using either WDM or TDM, but the signal must then be demultiplexed before regeneration.

All-optical regeneration by definition uses optical components to do the regeneration and has a significant potential in terms of the maxi-

mum bandwidth. However, in order to, e.g., restore the amplitude to the correct level, the regeneration process must be nonlinear, and this means that all-optical regeneration is inherently complex. Nevertheless a number of all-optical regenerators with promising performance have been demonstrated.

Regenerators are usually classified into one of three broad categories [54]. If only reamplification is carried out, the regenerator is classified as "1R". If, in addition to this, the pulses are also reshaped, i.e., the amplitude level and the pulse width are restored, the regenerator is denoted "2R". If the pulse is also moved to the centre of its corresponding bit slot, a process known as *retiming*, the regenerator is denoted "3R". A 3R regenerator must do clock recovery in order to have a time reference and is therefore more complicated, and in the following only 2R regenerators are considered.

Although it is possible to increase the signal quality with a regenerator, it is often not obvious how the improvement should be measured. The BER before and after regeneration cannot be used since no regenerator can increase the (local) BER. Instead, if the BER can be measured at chosen points inside the communication system, which is the case, e.g., when the dispersion is compensated for periodically, the BER is monotonically increasing with distance. This is pointed out in Ref. [54] and can be understood in the following way: If the BER is defined as the number of bit errors occurring in an optimised receiver, then also the regenerator will misinterpret the data. (Otherwise the receiver is not "optimised".) The regenerated pulse train can be of arbitrarily high quality but the bit errors will remain. The *final* BER can however be decreased by counteracting the accumulation of signal distortion, which, if left uncompensated, would eventually lead to bit errors.

For similar reasons it can be misleading to use the Q-value, since the intention behind this figure of merit is to relate easily measured quantities to the BER. Thus an increase in the Q-value might incorrectly lead to the conclusion that the BER is decreased. In the cases where the Q-value is used due to the lack of better suggestions, the fact that the impact on the final BER is hard to estimate must be remembered.

The fact that the noise statistics are significantly altered by a regenerator implies that it is generally hard to estimate the resulting BER. In the OOK case the Q-value is used to estimate the BER by assuming a Gaussian distribution for the noise, but such an assumption is likely to be incorrect in the case of a regenerated signal.

The regeneration process is different for different modulation formats, and it is, e.g., more complicated for DPSK data than for OOK data since in the former case the regenerator must adjust both the amplitude and the phase. Two separate descriptions follow, valid for OOK data and DPSK data, respectively, which are intended to put Papers F and G into proper context.

7.2 Regeneration of OOK data

In the case of RZ OOK data every bit is encoded as the presence or absence of a signal pulse. This means that a regenerator may reconstruct the pulse power without considering induced signal phase shifts, and OOK regeneration is therefore easier to accomplish than DPSK regeneration.

All-optical regeneration can be implemented using different kinds of nonlinear effects. A regenerator based on spectral widening by SPM and filtering was suggested by Mamyshev [55], and has been experimentally realised [56–58]. Pulse reshaping using soliton propagation in the regenerator is discussed in Ref. [30]. Strongly depleted FWM [59], Raman wavelength conversion [60], and fibre parametric amplification [61, 62], have also been used to achieve all-optical regeneration. Further examples of viable techniques include using a semiconductor optical amplifier (SOA) or a saturable absorber (SA) [54], or using a nonlinear optical-loop mirror (NOLM), see, e.g., Ref. [63]. However, the main topic of Paper F is the *Mamyshev regenerator* mentioned above, which implies that the focus will be on SPM-based regeneration.

Two different SPM-based regenerators have been simulated and compared in Ref. [64]. These regenerators use i) soliton-like pulse stabilisation and bandpass filtering and ii) SPM spectral broadening and bandpass filtering (Mamyshev regeneration). The experimental setups for these two types are similar. The differences are that the highly nonlinear fibre (HNLF) has anomalous dispersion in the case i) and normal dispersion in the case ii) and the bandpass filter is tuned to different centre frequencies, ω_0. In i) ω_0 is the frequency of the incoming signal, but in ii) it is detuned slightly to overlap with one of the main SPM lobes. The results show that both types are capable of increasing the transmission distance for pseudolinear systems, and that ii) is capable of better noise reduction and amplitude stabilisation but has a greater power loss than i).

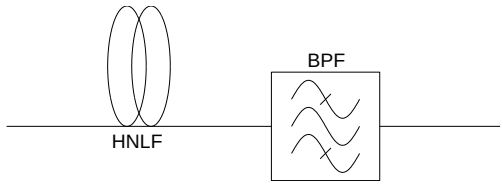

Figure 7.1: The regenerator consists of a HNLF followed by a bandpass filter.

Paper F presents a numerical study of the Mamyshev regenerator, which is plotted schematically in Fig. 7.1. Since the dispersive effects in the HNLF are small they have been neglected altogether in order to obtain a simpler system that can be completely described. Since the width of the regenerated pulse is determined by the filter bandwidth only two free parameters remain. These are the length of the HNLF and the centre frequency of the bandpass filter, ω_0, respectively.

The results show that amplitude regeneration and noise suppression are possible to obtain, but it is important to realise that there is a trade-off between these two effects; in order to obtain amplitude regeneration the spectra corresponding to the different input pulses must have similar amplitude at the frequency ω_0 and this is easier to obtain if the HNLF is short. On the other hand, to obtain good noise suppression the HNLF should be long in order to have small overlap between the (linear) noise pulse and the main SPM lobe. This is illustrated in Fig. 7.2 (taken from Paper F), in which the output peak power as a function of input peak power is plotted using different HNLF lengths. It is clearly seen that a long HNLF gives rise to strong noise suppression, but at the same time the curvature at the peak increases, implying that an interval in the input amplitude is mapped to a quite large interval in the output amplitude.

The main part of the results in Paper F were obtained using input pulses that were distorted by increasing the amplitude and decreasing the width (or vice versa) in such a way that the total energy is conserved. This is a reasonable assumption about the signal distortion effects in a communication link dominated by, e.g., PMD, but it is also interesting to study a case dominated by noise. This is also included in Paper F and the result here is slightly different. The noise floor in a bit slot carrying a zero can still be effectively suppressed but it is found that the amplitude jitter remains. This was found by studying pulses distorted by noise with a bandwidth equal to the pulse. (In this way only noise

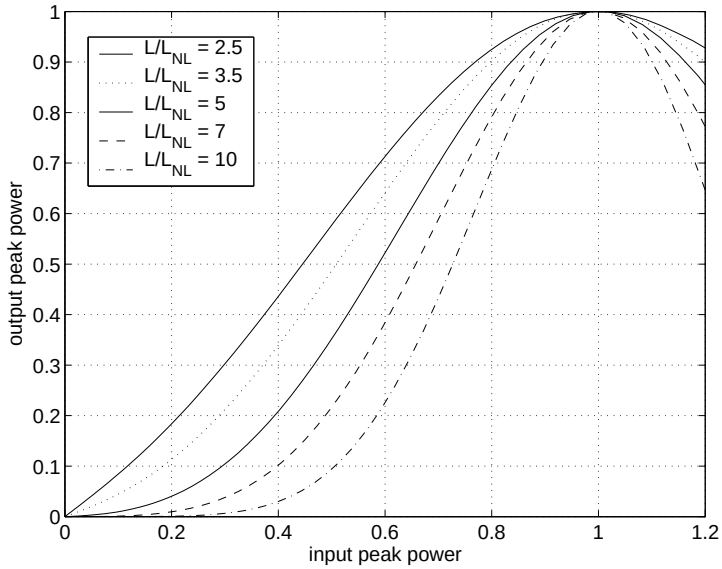

Figure 7.2: Peak power transmission of the pulse regenerator using $L/L_{NL} = 2.5, 3.5, 5, 7, 10$.

is included which cannot be removed by simple bandpass filtering.) On the other hand it was seen that ω_0 could be chosen in such a way that the amplitude jitter at least does not increase. Thus the above trade-off is modified and instead the focus is on the power loss in the regenerator. Numerical results in Paper F show how the energy transmission changes with the length of the HNLF, but using typical parameters it can be expected that between 10% and 25% of the pulse energy is transmitted by a Mamyshev regenerator.

7.3 Regeneration of DPSK data

In the DPSK DMF optical pulses are present in all bit slots, and the data is encoded as either 0 or π phase difference between neighbouring signal pulses [65]. Thus, the decoding of the pulse train depends on interference between neighbouring signal pulses in the receiver. In a *balanced receiver* the incoming pulse train is passed through a Mach–Zehnder delay interferometer (DI), which first splits the pulse train into two. One of these bit trains is then delayed an amount equivalent to the

bit slot and the two bit trains are joined, which causes them to interfere with each other. In this way the DI transforms the DPSK data into two OOK data streams which are complementary, i.e., one contains the data and one contains the logically negated data. By using two electronic receivers, that drive current in different directions, a symmetry is created which allows the decision threshold to be placed at zero.

An advantage of DPSK compared to OOK is the increased sensitivity; approximately 3 dB lower OSNR is required to obtain a given BER. The reason for this is that with the same average optical power, the symbol separation is $\sqrt{2}$ times larger for DPSK [1]. This advantage has been demonstrated by experimental results that have shown better performance for DPSK than for OOK in 40 Gbit/s systems [39]. The disadvantages include an increased experimental complexity and a sensitivity to phase distortions.

Regenerators designed for OOK data are usually not suited for DPSK data due to the introduction of phase distortion. One example is the Mamyshev regenerator which introduces significant and unacceptable phase shifts. This has lead to many suggestions of phase-preserving amplitude regenerators as a first step towards full DPSK regeneration. Examples of such systems are found in Ref. [66], which compares two of the amplitude regeneration schemes mentioned above; the first is self-regularisation using soliton propagation in the regenerator [30], and the second is amplitude stabilisation using FWM [61]. The results show that the regenerator based on FWM gives superior performance with virtually no induced phase distortion. A 2R DPSK regenerator using XPM which preserves the phase has been suggested [67], but the need for a reference synchronous pulse train makes the regenerator complicated. Furthermore a regenerator based on a NOLM has been suggested [68], but in order to achieve small phase distortion a directional attenuator has been included in the loop. Such a device is not trivial to realise and will cause unwanted power loss.

In order to regenerate the phase of a signal a phase reference is in principle needed to provide a known phase towards which the regenerator can adjust the phase. This can be achieved with an external phase reference or by using the signal as its own reference using averaging of the phase over several bit slots. The former principle is used in the case of phase-sensitive amplification [69], where degenerate FWM is used in a Mach–Zehnder interferometer with HNLF. The phase-sensitive amplification will force the signal value to either 0 or π depending on the initial

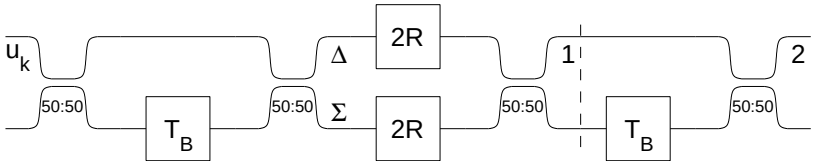

Figure 7.3: The regenerator consists of a DPSK receiver, two amplitude regenerators (marked "2R") and a coupler, which converts the data back into the DPSK modulation format.

phase difference between the pump and the signal. Operating the phase-sensitive amplifier in the undepleted region leads to almost perfect phase regeneration, but no amplitude regeneration. In the depleted region simultaneous amplitude and phase regeneration can be obtained, but in this case there will be a trade-off between the two effects. The obvious problem with this regeneration scheme is to set up the phase-locked pump signal, which must in some way be obtained using averaging of the phase in the propagated signal. An experimental verification of the results using the signal as a direct phase reference for the pump [70], confirms the phase-regenerative properties of this scheme.

An example of a regenerator based on averaging is the *semiconductor optical regenerative amplifier* (SORA) regenerator [71–73], which uses a SOA placed in the middle of a Sagnac loop. Two complementary OOK pulse trains are created using a DI of the same type as is used in a DPSK receiver. By making the travel time to the SOA identical, the one and the zero from the two pulse trains will meet each other in the SOA, and the zero will experience less gain because of gain depletion by the one. This leads to different gain for the one and the zero and increases the difference between the signal and noise power levels.

Paper G describes a DPSK regenerator which uses phase-preserving amplitude regenerators in a configuration shown in Fig. 7.3. Two OOK pulse trains are generated using a balanced DPSK receiver, and then amplitude regeneration is carried out. Finally, the OOK data is recombined into DPSK data again.

This regenerator is logically equivalent to the above described SORA. The regeneration in the SORA comes from the different gain for ones and zeroes, but in this case the method of regeneration is unspecified in order to study the system theoretically. In this way an upper limit for the phase regeneration that can be achieved with this type of regenerator

is found.

In Paper G a step-shaped transfer function is used as a model for the amplitude regenerators, i.e., the output amplitude is either a constant or zero depending on whether the incoming amplitude level is above a certain threshold. This type of regeneration can be considered ideal since no phase distortion is introduced and the output pulses have no amplitude jitter. However, the regenerated pulses are rectangular, i.e., the shape is significantly changed, but since the pulses are sampled in the middle of the bit slot this does not affect the results and alternative forms of ideal regeneration should give similar results. (It should however be noticed that the simple picture of an amplitude dependent transfer function for the pulse power that is used here is not valid for all types of regenerators. One example is the Mamyshev regenerator which mainly acts in Fourier space.)

As stated above it is not obvious how to measure the result of the regeneration. In Paper G the standard deviation of the phase error in the middle of the bit slot is used. This does not say anything about how the final BER is affected, but this is in general a difficult question which must be answered using direct numerical simulations or experiments. Nevertheless, the standard deviation provides a clear picture of the amount of phase error suppression.

The numerical result is easy to support with an analytical study of the system. Sufficient details are given in Paper G, but in summary the here considered regenerator (and the SORA) obtain the phase error suppression from averaging of the phase errors between two neighbouring pulses.

Unfortunately it is not easy to realise a regenerator of this type. The SORA is a proof-of-concept but the amplitude regeneration (based on differential gain) is not of high quality. As is discussed in Paper G the suppression of noise in bit slots carrying a zero is of critical importance for the phase-error suppression, and this is actually the main effect of the 2R regenerator in the SORA. However, no pulse reshaping is carried out, i.e., low amplitude jitter suppression will result. (The amplitude is averaged between neighbouring bit slots in the same way as it is done for the phase, and this suppresses the amplitude jitter to a certain extent.) The here considered regenerator provides good possibilities for separate regeneration of the two pulse trains, but practical regeneration schemes for the amplitude regenerators still need to be demonstrated.

Chapter 8

Conclusions

During the last decade the nonlinear intrachannel signal distortion in dispersion-managed optical communication systems operating in the pseudolinear regime has been carefully investigated and theoretically understood. The present thesis contributes to this development by analysing the phenomena of timing jitter, generation of ghost pulses, and amplitude jitter, and the results are relevant for the next generation optical networks. Both analytical and numerical methods have been used in order to obtain qualitative and quantitative understanding about these processes.

Timing jitter has been analysed separately, and the model equations have been interpreted in analogy with mechanics, which has provided good insight into the generation process. It has been described how the interaction strength changes during propagation and it has been found that the interaction is strongest for partially overlapping pulses. In a long pulse train with many pulses there is always partial overlap between some pulses, leading to almost linear growth of the timing jitter with propagation distance in the worst case. The strong suppressive effect from using suitable precompensation has been demonstrated.

Ghost pulses and amplitude jitter have been analysed by means of a perturbation analysis of the NLSE. This has clarified the generation and the dynamics of the nonlinear effects, and has made it possible to examine the different nonlinear effects individually. It has been found that the different contributions to the perturbation are frequency shifted, and their final temporal positions have been predicted analytically. An approximate expression has been derived for the contributions, which shows the dependence on the different system parameters clearly. Fur-

thermore the perturbation analysis has been used to predict the interaction range of the nonlinear effects. The effects from including attenuation and precompensation have also been described. The results for the perturbation can easily be modified to describe a system including ideal amplifiers and more general fibre parameters.

The nonlinear effects have been well understood and new means, beside numerical simulations of the NLSE, to predict the nonlinear behaviour of communication systems have been provided. This is important since the nonlinear effects are one of the limiting factors in present and future communication systems, and it is necessary to use proper modulation formats and suppression schemes to counteract them. Several suppression techniques have been described, and in particular two different schemes for phase shifting of the signal pulses, APRZ and PAP-RZ, have been demonstrated to have a suppressive effect.

All-optical regeneration has been discussed for both OOK and DPSK data. The SPM-based Mamyshev regenerator has been thoroughly investigated and it has, e.g., been shown that there is a trade-off between noise and amplitude jitter suppression. In the case of DPSK data a regenerator scheme that is equivalent to an already experimentally implemented regenerator has been examined. The results have shown how averaging between neighbouring pulses leads to the phase regeneration, and a prediction of the amount of phase-error suppression that can be achieved has been provided.

References

[1] P. J. Winzer and R.-J. Essiambre, "Advanced optical modulation formats", *Proceedings of the IEEE*, **94**, 5, 952–985, May 2006.

[2] G. P. Agrawal, *Fiber-Optic Communication Systems*, John Wiley & Sons, 2nd ed., 1997.

[3] G. P. Agrawal, *Nonlinear Fiber Optics*, Academic Press, 3rd ed., 2001.

[4] H. Sunnerud, *Polarization-Mode Dispersion in Optical Fibers: Characterization, Transmission Impairments, and Compensation*, Ph.D. thesis, Department of Microelectronics, Photonics Laboratory, Chalmers University of Technology, Göteborg, Sweden, 2001.

[5] S.-G. Park, A. H. Gnauck, J. M. Wiesenfeld, and L. D. Garrett, "40-Gb/s transmission over multiple 120-km spans of conventional single-mode fiber using highly dispersed pulses", *IEEE Photon. Technol. Lett.*, **12**, 8, 1085–1087, Aug 2000.

[6] B. Konrad and K. Petermann, "Optimum fiber dispersion in high-speed TDM systems", *IEEE Photon. Technol. Lett.*, **13**, 4, 299–301, April 2001.

[7] D. Breuer and K. Petermann, "Comparison of NRZ- and RZ-modulation format for 40-Gb/s TDM standard-fiber systems", *IEEE Photon. Technol. Lett.*, **9**, 3, 398–400, March 1997.

[8] M. I. Hayee and A. E. Willner, "NRZ versus RZ in 10-40-Gb/s dispersion-managed WDM transmission systems", *IEEE Photon. Technol. Lett.*, **11**, 8, 991–993, Aug 1999.

[9] I. Shake, H. Takara, K. Mori, et al., "Influence of inter-bit four-wave mixing in optical TDM transmission", *Electron. Lett.*, **34**, 16, 1600–1601, Aug 1998.

[10] R.-J. Essiambre, B. Mikkelsen, and G. Raybon, "Intra-channel cross-phase modulation and four-wave mixing in high-speed TDM systems", *Electron. Lett.*, **35**, 18, 1576–1578, Sept 1999.

[11] P. V. Mamyshev and N. A. Mamysheva, "Pulse-overlapped dispersion-managed data transmission and intrachannel four-wave mixing", *Opt. Lett.*, **24**, 21, 1454–1456, Nov 1999.

[12] M. Matsumoto, "Analysis of interaction between stretched pulses propagating in dispersion-managed fibers", *IEEE Photon. Technol. Lett.*, **10**, 3, 373–375, March 1998.

[13] S. Kumar, J. C. Mauro, S. Raghavan, and D. Q. Chowdhury, "Intrachannel nonlinear penalties in dispersion-managed transmission systems", *IEEE J. Select. Topics Quantum Electron.*, **8**, 3, 626–631, May/June 2002.

[14] A. Mecozzi, C. B. Clausen, M. Shtaif, et al., "Cancellation of timing and amplitude jitter in symmetric links using highly dispersed pulses", *IEEE Photon. Technol. Lett.*, **13**, 5, 445–447, May 2001.

[15] A. Mecozzi, C. B. Clausen, and M. Shtaif, "Analysis of intrachannel nonlinear effects in highly dispersed optical pulse transmission", *IEEE Photon. Technol. Lett.*, **12**, 4, 392–394, April 2000.

[16] M. J. Ablowitz and T. Hirooka, "Intrachannel pulse interactions in dispersion-managed transmission systems: Timing shifts", *Opt. Lett.*, **26**, 23, 1846–1848, Dec 2001.

[17] D. Anderson and M. Lisak, "Bandwidth limits due to incoherent soliton interaction in optical-fiber communication systems", *Phys. Rev. A*, **32**, 4, 2270–2274, Oct 1985.

[18] J. Mårtensson, M. Westlund, and A. Berntson, "Intra-channel pulse interactions in 40 Gbit/s dispersion-managed RZ transmission system", *Electron. Lett.*, **36**, 3, 244–246, Febr 2000.

[19] R. I. Killey, H. J. Thiele, V. Mikhailov, and P. Bayvel, "Reduction of intrachannel nonlinear distortion in 40-Gb/s-based WDM transmission over standard fiber", *IEEE Photon. Technol. Lett.*, **12**, 12, 1624–1626, Dec 2000.

[20] L. K. Wickham, R.-J. Essiambre, A. H. Gnauck, et al., "Bit pattern length dependence of intrachannel nonlinearities in pseudolinear transmission", *IEEE Photon. Technol. Lett.*, **16**, 6, 1591–1593, June 2004.

[21] A. G. Striegler and B. Schmauss, "Compensation of intrachannel effects in symmetric dispersion-managed transmission systems", *J. Lightw. Technol.*, **22**, 8, 1877–1882, Aug 2004.

[22] T. Inoue and A. Maruta, "Suppression of nonlinear intrachannel interactions between return-to-zero pulses in dispersion-managed optical transmission systems", *J. Opt. Soc. Am. B*, **19**, 3, 440–447, March 2002.

[23] A. Mecozzi, C. B. Clausen, and M. Shtaif, "System impact of intrachannel nonlinear effects in highly dispersed optical pulse transmission", *IEEE Photon. Technol. Lett.*, **12**, 12, 1633–1635, Dec 2000.

[24] M. J. Ablowitz and T. Hirooka, "Resonant nonlinear intrachannel interactions in strongly dispersion-managed transmission systems", *Opt. Lett.*, **25**, 24, 1750–1752, Dec 2000.

[25] M. J. Ablowitz and T. Hirooka, "Intrachannel pulse interactions in dispersion-managed transmission systems: Energy transfer", *Opt. Lett.*, **27**, 3, 203–205, Febr 2002.

[26] S. Kumar, "Intrachannel four-wave mixing in dispersion managed RZ systems", *IEEE Photon. Technol. Lett.*, **13**, 8, 800–802, Aug 2001.

[27] P. Johannisson, *Nonlinear impairment in strongly dispersion-managed optical communication systems*, Licentiate thesis, Chalmers University of Technology, Göteborg, Sweden, 2002.

[28] V. K. Mezentsev, S. K. Turitsyn, and N. J. Doran, "System optimisation of 80 Gbit/s single channel transmission over 1000 km of standard fibre", *Electron. Lett.*, **36**, 23, 1949–1951, Nov 2000.

[29] J. Mårtensson, A. Berntson, M. Westlund, et al., "Timing jitter owing to intrachannel pulse interactions in dispersion-managed transmission systems", *Opt. Lett.*, **26**, 2, 55–57, Jan 2001.

[30] M. Matsumoto and O. Leclerc, "Analysis of 2R optical regenerator utilising self-phase modulation in highly nonlinear fibre", *Electron. Lett.*, **38**, 12, 576–577, June 2002.

[31] M. Forzati, J. Mårtensson, A. Berntson, et al., "Reduction of intrachannel four-wave mixing using the alternate-phase RZ modulation format", *IEEE Photon. Technol. Lett.*, **14**, 9, 1285–1287, Sept 2002.

[32] B. Konrad, K. Petermann, J. Berger, et al., "Impact of fiber chromatic dispersion in high-speed TDM transmission systems", *J. Lightw. Technol.*, **20**, 12, 2129–2135, Dec 2002.

[33] M. Forzati, A. Berntson, and J. Mårtensson, "IFWM suppression using APRZ with optimized phase-modulation parameters", *IEEE Photon. Technol. Lett.*, **16**, 10, 2368–2370, Oct 2004.

[34] S. Randel, B. Konrad, A. Hodžić, and K. Petermann, "Influence of bitwise phase changes on the performance of 160 Gbit/s transmission systems", in *Proc. of European Conference on Optical Communication (ECOC 2002)*, P3.31, Sept 2002.

[35] Y. Miyamoto, A. Hirano, K. Yonenaga, et al., "320 Gbit/s (8×40 Gbit/s) WDM transmission over 367 km zero-dispersion-flattened line with 120 km repeater spacing using carrier-suppressed return-to-zero pulse format", *Electron. Lett.*, **35**, 23, 2041–2042, Nov 1999.

[36] K. Yonenaga, Y. Miyamoto, A. Hirano, et al., "320 Gbit/s WDM field experiment using 40 Gbit/s ETDM channels over 176 km dispersion-shifted fibre with nonlinearity-tolerant signal format", *Electron. Lett.*, **36**, 2, 153–155, Jan 2000.

[37] D. Dahan and G. Eisenstein, "Numerical comparison between distributed and discrete amplification in a point-to-point 40-Gb/s 40-WDM-based transmission system with three different modulation formats", *J. Lightw. Technol.*, **20**, 3, 379–388, March 2002.

[38] A. Hodžić, B. Konrad, and K. Petermann, "Alternative modulation formats in $N \times 40$ Gb/s WDM standard fiber RZ-transmission systems", *J. Lightw. Technol.*, **20**, 4, 598–607, April 2002.

[39] A. H. Gnauck, X. Liu, X. Wei, et al., "Comparison of modulation formats for 42.7-Gb/s single-channel transmission through 1980 km

of SSMF", *IEEE Photon. Technol. Lett.*, **16**, 3, 909–911, March 2004.

[40] R. Ohhira, D. Ogasahara, and T. Ono, "Novel RZ signal format with alternate-chirp for suppression of nonlinear degradation in 40 Gb/s based WDM", in *Optical Fiber Communication Conference (OFC2001)*, WM2:1–WM2:3, 2001.

[41] B. Bakhshi, M. Vaa, E. A. Golovchenko, et al., "Comparison of CRZ, RZ and NRZ modulation formats in a 64×12.3 Gb/s WDM transmission experiment over 9000 km", in *Optical Fiber Communication Conference (OFC2001)*, WF4:1–WF4:3, 2001.

[42] A. Sano and Y. Miyamoto, "Performance evaluation of prechirped RZ and CS-RZ formats in high-speed transmission systems with dispersion management", *J. Lightw. Technol.*, **19**, 12, 1864–1871, Dec 2001.

[43] K. S. Cheng and J. Conradi, "Reduction of pulse-to-pulse interaction using alternative RZ formats in 40-Gb/s systems", *IEEE Photon. Technol. Lett.*, **14**, 1, 98–100, Jan 2002.

[44] X. Liu, X. Wei, A. H. Gnauck, et al., "Suppression of intrachannel four-wave-mixinginduced ghost pulses in high-speed transmissions by phase inversion between adjacent marker blocks", *Opt. Lett.*, **27**, 13, 1177–1179, July 2002.

[45] P. J. Winzer, A. H. Gnauck, G. Raybon, et al., "40-Gb/s return-to-zero alternate-mark-inversion (RZ-AMI) transmission over 2000 km", *IEEE Photon. Technol. Lett.*, **15**, 5, 766–768, May 2003.

[46] G.-W. Lu, L.-K. Chen, and C.-K. Chan, "A simple AMI-RZ transmitter based on single-arm intensity modulator and optical delay interferometer", *Opt. Commun.*, **255**, 1-3, 35–40, Nov 2005.

[47] D. M. Gill, A. H. Gnauck, X. Liu, et al., "$\pi/2$ alternate-phase ON-OFF keyed 40-Gb/s transmission on standard single-mode fiber", *IEEE Photon. Technol. Lett.*, **15**, 12, 1776–1778, Dec 2003.

[48] D. M. Gill, A. H. Gnauck, X. Liu, et al., "$\pi/2$ alternate-phase on-off keyed 42.7 Gb/s long-haul transmission over 1980 km of standard single-mode fiber", *IEEE Photon. Technol. Lett.*, **16**, 3, 906–908, March 2004.

[49] S. Appathurai, V. Mikhailov, R. I. Killey, and P. Bayvel, "Effective suppression of intra-channel nonlinear distortion in 40 Gbit/s transmission over standard singlemode fibre using alternate-phase RZ and alternate polarisation", *Electron. Lett.*, **40**, 14, 897–898, July 2004.

[50] J. Mårtensson, J. Li, A. Berntson, et al., "Suppression of intra-channel four-wave mixing by phase-modulation at one quarter of bit rate", *Electron. Lett.*, **38**, 23, 1463–1465, Nov 2002.

[51] N. Alić and Y. Fainman, "Data-dependent phase coding for suppression of ghost pulses in optical fibers", *IEEE Photon. Technol. Lett.*, **16**, 4, 1212–1214, April 2004.

[52] B. Vasic, V. S. Rao, I. B. Djordjevic, et al., "Ghost-pulse reduction in 40-Gb/s systems using line coding", *IEEE Photon. Technol. Lett.*, **16**, 7, 1784–1786, July 2004.

[53] J. Zweck and C. R. Menyuk, "Analysis of four-wave mixing between pulses in high-data-rate quasi-linear subchannel-multiplexed systems", *Opt. Lett.*, **27**, 14, 1235–1237, July 2002.

[54] O. Leclerc, B. Lavigne, E. Balmefrezol, et al., "Optical regeneration at 40 Gb/s and beyond", *J. Lightw. Technol.*, **21**, 11, 2779–2789, Nov 2003.

[55] P. V. Mamyshev, "All-optical data regeneration based on self-phase modulation effect", in *Proc. of European Conference on Optical Communication (ECOC 1998)*, 475–476, Sept 1998.

[56] B.-E. Olsson and D. J. Blumenthal, "Pulse restoration by filtering of self-phase modulation broadened optical spectrum", *J. Lightw. Technol.*, **20**, 7, 1113–1117, July 2002.

[57] G. Raybon, Y. Su, J. Leuthold, et al., "40 Gbit/s pseudo-linear transmission over one million kilometers", in *Optical Fiber Communication Conference (OFC2002)*, FD10:1–FD10:3, 2002, post-deadline paper.

[58] Y. Su, G. Raybon, R.-J. Essiambre, and T.-H. Her, "All-optical 2R regeneration of 40-Gb/s signal impaired by intrachannel four-wave mixing", *IEEE Photon. Technol. Lett.*, **15**, 2, 350–352, Febr 2003.

[59] E. Ciaramella and S. Trillo, "All-optical signal reshaping via four-wave mixing in optical fibers", *IEEE Photon. Technol. Lett.*, **12**, 7, 849–851, July 2000.

[60] D. Dahan, R. Alizon, A. Bilenca, and G. Eisenstein, "Optical noise reduction in inter-band Raman mediated wavelength conversion", *Electron. Lett.*, **39**, 3, 307–309, Febr 2003.

[61] K. Inone, "Optical level equalisation based on gain saturation in fibre optical parametric amplifier", *Electron. Lett.*, **36**, 12, 1016–1017, June 2000.

[62] Y. Li, K. Croussore, C. Kim, and G. Li, "All-optical 2R regeneration using data-pumped fibre parametric amplification", *Electron. Lett.*, **39**, 17, 1263–1264, Aug 2003.

[63] S. Bigo, O. Leclerc, and E. Desurvire, "All-optical fiber signal processing and regeneration for soliton communications", *IEEE J. Select. Topics Quantum Electron.*, **3**, 5, 1208–1223, Oct 1997.

[64] M. Matsumoto, "Performance analysis and comparison of optical 3R regenerators utilizing self-phase modulation in fibers", *J. Lightw. Technol.*, **22**, 6, 1472–1482, June 2004.

[65] A. H. Gnauck and P. J. Winzer, "Optical phase-shift-keyed transmission", *J. Lightw. Technol.*, **23**, 1, 115–130, Jan 2005.

[66] M. Matsumoto, "Regeneration of RZ-DPSK signals by fiber-based all-optical regenerators", *IEEE Photon. Technol. Lett.*, **17**, 5, 1055–1057, May 2005.

[67] A. Striegler and B. Schmauss, "All-optical DPSK signal regeneration based on cross-phase modulation", *IEEE Photon. Technol. Lett.*, **16**, 4, 1083–1085, April 2004.

[68] A. G. Striegler, M. Meissner, K. Cveček, et al., "NOLM-based RZ-DPSK signal regeneration", *IEEE Photon. Technol. Lett.*, **17**, 3, 639–641, March 2005.

[69] K. Croussore, C. Kim, and G. Li, "All-optical regeneration of differential phase-shift keying signals based on phase-sensitive amplification", *Opt. Lett.*, **29**, 20, 2357–2359, Oct 2004.

[70] K. Croussore, I. Kim, Y. Han, et al., "Demonstration of phase-regeneration of DPSK signals based on phase-sensitive amplification", *Opt. Express*, **13**, 11, 3945–3950, May 2005.

[71] V. S. Grigoryan, M. Shin, P. Devgan, and P. Kumar, "Mechanism of SOA-based regenerative amplification of phase-noise degraded DPSK signals", *Electron. Lett.*, **41**, 18, 1021–1022, Sept 2005.

[72] M. Shin, P. S. Devgan, V. S. Grigoryan, and P. Kumar, "SNR improvement of DPSK signals in a semiconductor optical regenerative amplifier", *IEEE Photon. Technol. Lett.*, **18**, 1, 49–51, Jan 2006.

[73] V. S. Grigoryan, M. Shin, P. Devgan, et al., "SOA-based regenerative amplification of phase-noise-degraded DPSK signals: Dynamic analysis and demonstration", *J. Lightw. Technol.*, **24**, 1, 135–142, Jan 2006.

Included papers A–G

Paper A

J. Mårtensson, A. Berntson, M. Westlund, A. Danielsson, P. Johannisson, D. Anderson, and M. Lisak, "Timing jitter owing to intrachannel pulse interactions in dispersion-managed transmission systems", *Opt. Lett.*, **26**, 2, 55–57, Jan 2001.

Paper B

P. Johannisson, D. Anderson, A. Berntson, and J. Mårtensson, "Generation and dynamics of ghost pulses in strongly dispersion-managed fiber-optic communication systems", *Opt. Lett.*, **26**, 16, 1227–1229, Aug 2001.

Paper C

P. Johannisson, "Interaction range and generation rate of nonlinear intrachannel signal distortion", *submitted to J. Opt. Soc. Am. B*, 2006.

Paper D

P. Johannisson, D. Anderson, M. Marklund, A. Berntson, M. Forzati, and J. Mårtensson, "Suppression of nonlinear effects by phase alternation in strongly dispersion-managed optical transmission", *Opt. Lett.*, **27**, 12, 1073–1075, June 2002.

Paper E

M. Forzati, J. Mårtensson, A. Berntson, A. Djupsjöbacka, and P. Johannisson, "Reduction of intrachannel four-wave mixing using the alternate-phase RZ modulation format", *IEEE Photon. Technol. Lett.*, **14**, 9, 1285–1287, Sept 2002.

Paper F

P. Johannisson and M. Karlsson, "Characterization of a self-phase-modulation-based all-optical regeneration system", *IEEE Photon. Technol. Lett.*, **17**, 12, 2667–2669, Dec 2005.

Paper G

P. Johannisson, G. Adolfsson, and M. Karlsson, "Suppression of phase error in differential phase-shift keying data by amplitude regeneration", *Opt. Lett.*, **31**, 10, 1385–1387, May 2006.